

# Generalized Decoupled Learning for Enhancing Open-Vocabulary Dense Perception

Junjie Wang, Keyu Chen, Yulin Li, Bin Chen, Hengshuang Zhao, Xiaojuan Qi, Zhuotao Tian



Fig. 1: **Illustration of the proposed DeCLIP method.** DeCLIP adopts a decoupled learning strategy to enhance pixel-level open-vocabulary representations, which can serve as a general foundation model for OV dense perception tasks such as 2D detection and segmentation (including training-free segmentation), 3D instance segmentation, video instance segmentation, and 6D object pose estimation.

**Abstract**—Dense visual perception tasks have been constrained by their reliance on predefined categories, limiting their applicability in real-world scenarios where visual concepts are unbounded. While Vision-Language Models (VLMs) like CLIP have shown promise in open-vocabulary tasks, their direct application to dense perception often leads to suboptimal performance due to limitations in local feature representation. In this work, we present our observation that CLIP’s image tokens struggle to effectively aggregate information from spatially or semantically related regions, resulting in features that lack local discriminability and spatial consistency. To address this issue, we propose DeCLIP, a novel framework that enhances CLIP by decoupling the self-attention module to obtain “content” and “context” features respectively. The context features are enhanced by jointly distilling semantic correlations from Vision Foundation Models (VFM) and object integrity cues from diffusion models, thereby enhancing spatial consistency. In parallel, the content features are aligned with image crop

representations and constrained by region correlations from VFMs to improve local discriminability. Extensive experiments demonstrate that DeCLIP establishes a solid foundation for open-vocabulary dense perception, consistently achieving state-of-the-art performance across a broad spectrum of tasks, including 2D detection and segmentation, 3D instance segmentation, video instance segmentation, and 6D object pose estimation. Code is available at <https://github.com/xiaomoguhz/DeCLIP>

**Index Terms**—Dense Perception, Open-Vocabulary, Scene Understanding, 2D/3D Segmentation.

## 1. INTRODUCTION

IN the era of deep learning, dense perception tasks like object detection [1], [2] and image segmentation [3], [4] have rapidly advanced and are widely used. However, traditional methods [5]–[7] recognize only a fixed set of predefined categories. This restriction hinders the practical application of these methods in real-world settings, where the range of visual concepts is virtually boundless. Consequently, increasing attention has been drawn to OV (Open-Vocabulary) methods [8]–[11], which aim to detect and segment objects from any category using textual descriptions.

Junjie Wang, Keyu Chen, Yulin Li, Bin Chen, and Zhuotao Tian are with the Harbin Institute of Technology (Shenzhen). Hengshuang Zhao and Xiaojuan Qi are with the University of Hong Kong. E-mail: jjwanghz@stu.hit.edu.cn (Junjie Wang)

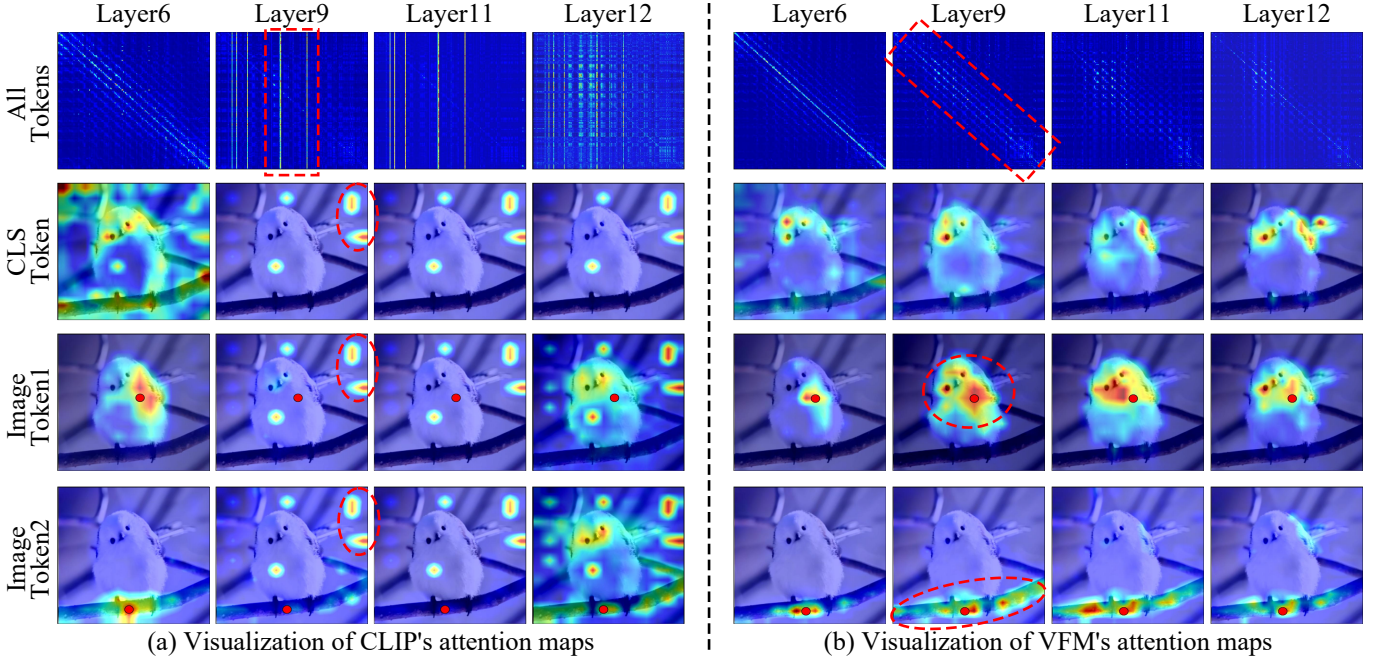


Fig. 2: **Comparison of the attention patterns of CLIP and VFM across different layers.** The attention weights of CLIP and VFM are collected at various layers, averaged across the head dimension, and upsampled to the original resolution for visualization. The first row presents the visualization of attention weights for all tokens. The second, third, and fourth rows utilize the [CLS] token and image tokens at different positions as queries, respectively, to illustrate their attention distributions to other tokens. The selected query image tokens are indicated with red dots. We observed significant differences in the deep-layer attention patterns between CLIP and VFM. The attention of VFM’s image tokens consistently focuses on semantically relevant regions. In contrast, CLIP’s attention abruptly focuses on several specific tokens in the deeper layers, which may be the primary reason for its inferior performance in dense perception tasks.

Building on the success of Vision-Language Models (VLMs) [12], [13] pre-trained on image-text pairs, such as CLIP [12], researchers have extended these models to OV dense perception tasks [14], [15]. To apply CLIP to such tasks, various method paradigms have been explored, including pseudo-labeling [16], [17], knowledge distillation [18], and transfer learning [19], [20]. Leveraging CLIP as the foundation provides significant advantages due to its comprehensive pre-training. However, directly applying these image-level models to dense prediction tasks often leads to domain shift issues, which degrades performance [10].

**What Hinders CLIP in Dense Perception?** To assess CLIP’s constraints in dense perception, we first analyze the discrepancies in attention maps across multiple layers between CLIP and VFM (Vision Foundation Model). The latter is known to excel in dense perception tasks. As shown in Fig. 2, our experiments reveal that CLIP’s [CLS] token may interfere with the correlations among other image tokens, leading to suboptimal performance in dense perception tasks.

**Emerging Differences in Deep-Layer Attention.** We observe significant differences in attention maps between CLIP and VFMs begin to emerge from the 9th layer onward. Specifically, in deeper layers, CLIP’s [CLS] token shifts focus away from primary objects within the image and attends highly to certain specific tokens, as highlighted by the red dashed circle in the 2nd row of Fig. 2(a). Moreover, CLIP’s image tokens

(rows 3 and 4, Fig. 2(a)) exhibit similar behavior to the [CLS] token, showing high attention to several specific tokens rather than semantically related regions, regardless of their positions. In contrast, VFM’s image tokens consistently focus on semantically relevant regions from shallow to deep layers.

This observation sheds light on why CLIP struggles in dense perception tasks: its image tokens fail to aggregate information from semantically related regions, resulting in dense features that lack local discriminability and spatial consistency<sup>1</sup>. As shown in Fig. 3(b), directly using CLIP features on the COCO dataset yields inferior performance in object detection and semantic segmentation. To tackle this, an intuitive approach is to enhance CLIP’s local representations through fine-tuning. However, balancing the optimizations of both dense feature spatial correlations and vision-language semantic alignment within a unified architecture becomes a new challenge. Therefore, *is it feasible to disentangle CLIP’s features and apply separate guiding constraints to obtain diverse features within a unified architecture?*

**Our Solution.** To address these challenges, we propose DeCLIP, a general unsupervised fine-tuning method aimed at enhancing both the discriminability and spatial consistency of CLIP’s local features. The core idea is to decouple the self-

<sup>1</sup>Local discriminability refers to a model’s ability to distinguish semantics between objects, while spatial consistency means semantics within an object remain coherent, similar, and clearly bounded.



attention module of CLIP and learn from different teacher models separately.

Specifically, DeCLIP decouples the features in the self-attention module into “content” and “context” components. The “content” features, responsible for local discriminability, are fine-tuned by aligning pooled region features with their corresponding image crop [CLS] representations. Meanwhile, the “context” features, responsible for spatial consistency, are learned from the feature correlations generated by VFMs. This decoupled distillation design effectively mitigates optimization conflicts, improving the generalization ability when applying CLIP to downstream OV dense perception tasks.

In addition, we observe that the semantic affinity maps of VFM (i.e., the teacher signals for context features) lack object integrity, such as unclear object boundaries and internal holes. To address this, we leverage self-attention maps from the Stable Diffusion (SD) [21] to enhance semantic completeness. Additionally, we find that aligning content features with [CLS] representations weakens CLIP’s dense correlations, prompting us to use regional correlations from VFM as a constraint. These enhancements further improve the fine-grained perceptual capability. As shown in Fig 3, DeCLIP significantly outperforms CLIP in dense perception tasks.

To summarize, our contributions are as follows:

- Through a comparative analysis of the attention maps of CLIP and VFM, we identified that CLIP’s inferior performance in dense perception tasks stems from its image tokens failing to attend to semantically relevant regions in the deep layers.
- To address this issue, we propose DeCLIP, an effective unsupervised fine-tuning framework, to enhance the discriminability and spatial consistency of CLIP’s dense features via a decoupled feature enhancement strategy.
- As illustrated in Fig. 3(a), extensive experiments demonstrate that DeCLIP can be applied to various tasks, including 2D detection/segmentation, 3D instance segmentation, and video instance segmentation. These results highlight its potential to serve as a foundation model for OV dense perception tasks.

## 2. RELATED WORKS

### 2.1 Open-Vocabulary Dense Perception

OV dense perception aims to achieve fine-grained classification of arbitrary visual instances by leveraging textual descriptions [22], [23]. According to the structure and dimensionality of the input data, the tasks can be categorized into the following three typical scenarios:

**2D Dense Perception.** This scenario takes RGB images as input, with typical tasks such as object detection [9], [24] and image segmentation [19], [25], [26]. 2D OV dense perception methods based on pretrained CLIP can generally be categorized into pseudo-labeling [16], [27], [28], knowledge distillation [24], [29], [30], and transfer learning [15], [17], [19]. Regardless of the approach, these methods heavily rely on CLIP’s dense perception capabilities. For instance, [16] produces region-text pseudo-labels using CLIP’s regional features. [15], [19] employ CLIP’s image encoder as the backbone

and train task-specific detection or segmentation components upon it. Clearly, these methods are inherently limited by the quality of CLIP’s dense features.

**3D Dense Perception.** Beyond 2D images, OV fine-grained perception can be extended to 3D scenes, enabling instance segmentation [31]–[34] or object pose estimation [35] on point cloud and RGB-D data. The challenges faced in 3D scenes are similar to those in 2D. Since CLIP itself lacks the ability to process 3D data, existing methods typically project 3D data into 2D RGB images from different viewpoints for OV instance recognition [36], [37], then fuse the results from multiple viewpoints to achieve 3D instance segmentation.

**Video Dense Perception.** In addition to static 2D and 3D scenarios, OV dense perception can also be applied to video sequences, facilitating video instance segmentation [38]–[40]. In video scenarios, CLIP is often used to extract features for single-frame images, which are then pooled with masks to construct memory banks for multi-frame consistency tracking [38]. The quality of CLIP’s dense features directly affects the accuracy of single-frame instance segmentation and the effectiveness of the memory bank.

Therefore, whether for 2D, 3D, or video scenarios, CLIP’s dense perception capability is critical. To address this, this paper proposes a decoupled feature enhancement strategy to improve the spatial consistency and discriminability of CLIP’s dense features, and comprehensively evaluates the effectiveness of the proposed method across the aforementioned tasks.

### 2.2 Adapting CLIP to Dense Perception Tasks.

Since VLMs [12], [41] are initially trained on image-text pairs, directly applying these image-level models to dense perception tasks, which require region-level or pixel-level semantic understanding, often results in significant performance degradation. Several studies have attempted to mitigate the domain shift problem encountered when applying CLIP to such tasks. These approaches can be broadly categorized into three main groups:

**Joint Fine-Tuning.** These methods fine-tune CLIP while training task-specific components [11], [20], [42], [43]. For instance, OV semantic segmentation method CAT-Seg [11] proposes an attention fine-tuning strategy based on ViT CLIP, which generalizes well to unseen categories. MAFT [42] proposes a mask-aware fine-tuning strategy, which enhances CLIP’s sensitivity to mask proposals while maintaining its transferability to unseen categories.

**Pre-Fine-Tuning.** These methods directly fine-tune CLIP using cost-efficient techniques [15], [16], [44]. For instance, CLIM [14] employs a mosaic augmentation technique to stitch multiple images into a single image, enabling each sub-image to serve as a pseudo-region for region-text contrastive learning. As illustrated in Fig. 4(b), CLIPSelf [15] enhances CLIP’s region classification accuracy by maximizing cosine similarity between its region representations and the corresponding image crop representations.

**Combining CLIP with VFMs.** These studies [45]–[47] investigate the integration of CLIP with VFMs. For instance,

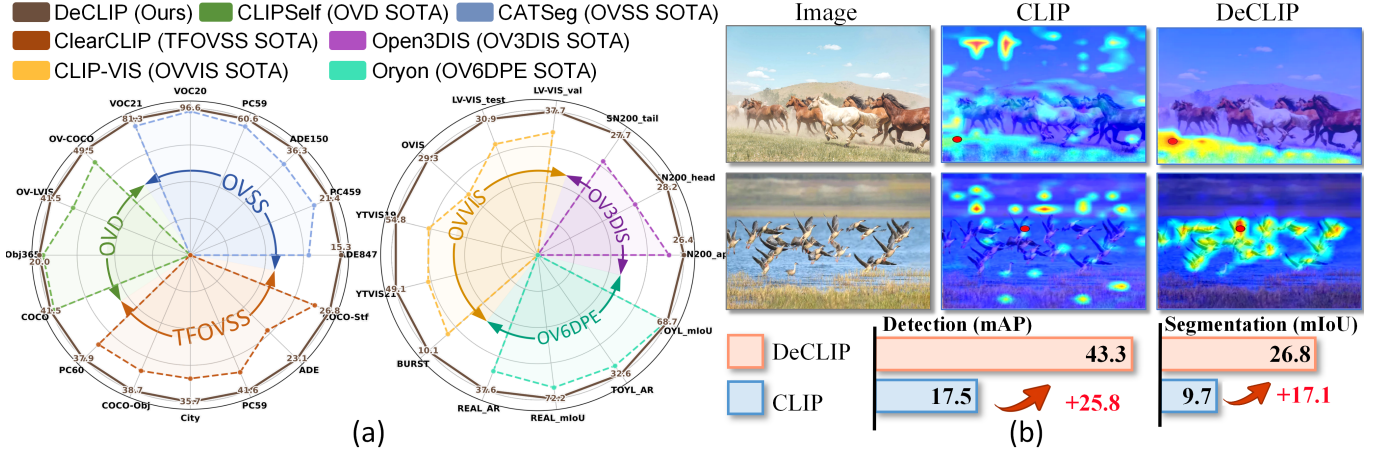


Fig. 3: (a) **Comparison between DeCLIP and state-of-the-art methods across six OV dense perception tasks.** These tasks include OV detection and semantic segmentation (OVD, OVSS), training-free OV semantic segmentation (TFOVSS), OV 3D and video instance segmentation (OV3DIS, OVVIS), and OV 6D pose estimation (OV6DPE). Experiments demonstrate the effectiveness of DeCLIP as a foundation model for OV dense perception. (b) **Quantitative and qualitative comparisons between DeCLIP and CLIP.** Compared to CLIP, DeCLIP’s image tokens attend to semantically relevant regions of query tokens, significantly improving dense perception performance. The query tokens are highlighted by red dots.

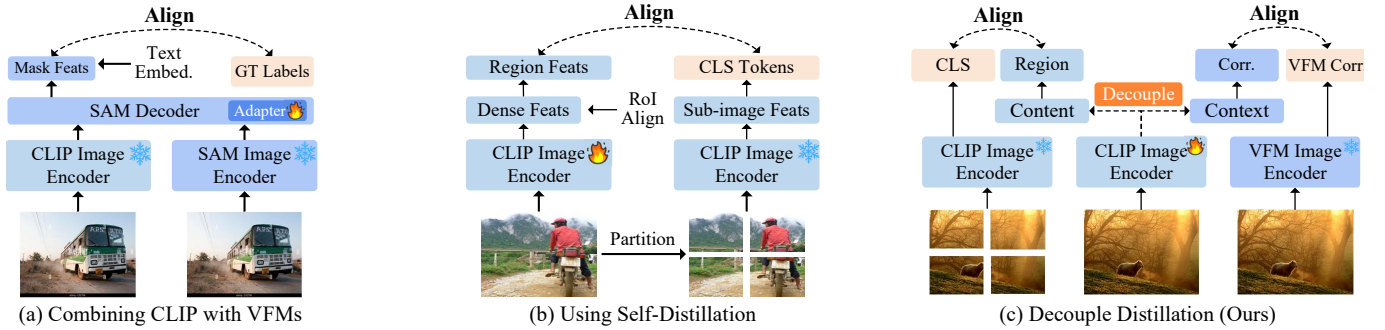


Fig. 4: **Comparison between DeCLIP and existing related methods.** (a) Methods that combine CLIP with VFMs typically integrate CLIP into SAM and transform it into an OV segmenter, which often requires costly dense annotations to train adapters. (b) Pre-fine-tuning methods adapt CLIP in a cost-effective manner, for example, by aligning CLIP’s local features with the CLS tokens of corresponding sub-images. However, these methods still fail to apply to image segmentation tasks. (c) Our DeCLIP enhances dense features’ local discriminability and spatial consistency via the content-context decoupled learning, enabling a unified OV dense perception foundation model.

SAM-CLIP [45], OV-SAM [46], and FrozenSeg [47] seek to combine the advanced image segmentation capabilities of SAM [48] with the zero-shot semantic understanding capabilities of CLIP, as illustrated in Fig. 4(a).

Despite the promising results of the three categories of methods, they continue to exhibit certain limitations. Joint fine-tuning methods are typically specific to tasks or models and heavily rely on labor-intensive annotations of dense perception tasks. Pre-fine-tuning methods demonstrate broader applicability. However, their region-level fine-tuning technique remains limited in image segmentation tasks that require pixel-level details. Methods that combine CLIP with VFMs mainly focus on integrating CLIP into SAM or distilling them into a multi-task model, rather than enhancing CLIP itself as DeCLIP does. Notably, recent advances [49] in image generation have also explored using VFM to enhance local representations. In contrast, DeCLIP introduces an innovative

decoupled distillation strategy, as shown in Fig. 4(c).

### 3. BACKGROUND AND MOTIVATION

#### 3.1 Preliminaries

**Contrastive Language-Image Pre-training (CLIP)** [12] is built upon two encoders, one for images and one for text. The visual encoder can be a CNN series [50], [51] or ViT [52], and the text encoder is a Transformer [53]. This paper focuses on CLIP with the ViT architecture, which adopts the [CLS] token to represent the overall features of an image. CLIP learns vision-language alignment by maximizing the cosine similarity between the [CLS] token and text features of matched image-text pairs, and minimizing the similarity for unmatched pairs.

**Dense Feature Extraction with CLIP.** ViT-based CLIP consists of a series of stacked attention blocks. For example, the ViT-B version of CLIP includes 12 attention block layers.



Let  $\mathbf{X} = \{\mathbf{x}_0, \mathbf{x}_1, \dots, \mathbf{x}_{h \times w}\}$  denotes the input to the last attention block, where  $\mathbf{x}_i \in \mathbb{R}^{1 \times D}$ . The computation within this attention block can be expressed as:

$$\mathbf{Q} = \text{Proj}_q(\mathbf{X}), \mathbf{K} = \text{Proj}_k(\mathbf{X}), \mathbf{V} = \text{Proj}_v(\mathbf{X}), \quad (1)$$

$$\mathbf{Y} = \mathbf{X} + \text{Proj}(\text{Attn}_{qk} \cdot \mathbf{V}), \quad (2)$$

$$\mathbf{Z} = \mathbf{Y} + \text{FFN}(\mathbf{Y}), \quad (3)$$

where  $\mathbf{Q}$ ,  $\mathbf{K}$ , and  $\mathbf{V}$  represent the query, key, and value embeddings, respectively;  $\text{Proj}$  denotes projection layers;  $\text{Attn}_{qk} = \text{SoftMax}(\mathbf{Q}\mathbf{K}^\top / \sqrt{d})$  represents the self-attention process, with  $d$  denoting the dimension of each attention head.  $\text{FFN}$  denotes a feed-forward network. For simplicity, normalization operations are omitted. After passing through the final attention block,  $\mathbf{Z}[0]$  represents the global [CLS] token. The remaining image patch embeddings  $\mathbf{Z}[1 : h \times w]$  can be reshaped to obtain dense feature representations  $\mathbf{X}_{\text{dense}} \in \mathbb{R}^{C \times H \times W^2}$ .

### 3.2 Key Observations

In Sec. 2.1, we discuss the significance of CLIP’s dense perception capability for various OV tasks. In Sec. 2.2, we analyze the limitations of existing methods for adapting CLIP features to dense perception tasks. To address the limitations of existing approaches and to gain deeper insight into the intrinsic challenges associated with applying CLIP representations to dense perception tasks, we first analyze the differences in attention maps across different layers of CLIP and VFM.

**Dense Correlations in CLIP’s Early Layers.** As shown in the first column of Fig. 2(a), we observe that in the shallow layers of CLIP (e.g., layer 6), the [CLS] token’s attention is broadly distributed across the image. From the viewpoint of image tokens, the attention weights of each image token primarily focus on semantically relevant regions. The overall attention pattern at this stage exhibits locality, with the highlighted attention regions mainly distributed along the diagonal.

**Vanishing Correlations in CLIP’s Deep Layers.** As illustrated in the second column of Fig. 2(a), a notable shift in the attention patterns is observed in the deeper layers of CLIP. Specifically, in the deeper layers (e.g., layer 9), the [CLS] token shifts its focus away from the primary objects in the image and attends to several specific tokens, as indicated by the red dashed circles. For clarity, we refer to these special tokens as “proxy tokens”. These specific tokens may serve as “proxies” for the [CLS] token. This suggests that these tokens aggregate essential information from other image tokens, enabling the [CLS] token to form an approximate “global view” by summarizing their content, thereby facilitating image classification. However, these “proxy tokens” may negatively affect the attention patterns of CLIP’s image tokens.

In particular, when the [CLS] token focuses on the proxy tokens, CLIP’s image tokens similarly shift their attention to these special tokens instead of semantically or spatially relevant regions. Furthermore, when the visualization position of the query image token is altered (from the bird to the branch, fourth row of Fig. 2(a)), we observe that the new

TABLE 1: Performance of different distillation schemes.

Distillation Type	Region Classification (mAcc)		Semantic Segmentation (mIoU)	
	COCO (Thing)	COCO (Stuff)	Context59	CityScape
Self-Distillation [15]	69.5	44.6	29.4	25.6
Self+VFM Distillation [48]	65.6 (-3.9)	41.3 (-3.3)	32.4 (+3.0)	28.7 (+3.1)
Self+VFM+Decouple	75.0 (+5.5)	51.8 (+7.2)	35.3 (+5.9)	32.3 (+6.7)

query image token continues to assign high attention to the “proxy tokens.” Notably, we observe that all image tokens at this stage exhibit this global attention pattern, with the highlighted attention regions manifesting as several prominent vertical lines (first row, Fig. 2(a)).

**VFM Exhibits Consistent Dense Correlations.** Considering the inherent constraints that impede CLIP’s efficacy in dense perception tasks, we instead observe that VFMs such as the DINO series [54], [55], trained in a self-supervised learning (SSL), and the SAM series [48], [56], trained on large-scale segmentation data, are capable of extracting features with strong spatial consistency, as shown in Fig. 2(b).

In particular, the attention maps of VFMs do not exhibit the “proxy token” phenomenon observed in CLIP. Furthermore, we observe that the image tokens of VFMs consistently focus on semantically relevant regions from shallow to deep layers (i.e., third and fourth rows, Fig. 2(b)). In contrast, the image tokens of CLIP lose these dense correlations in the deeper layers. This results in a lack of correlation between image tokens that share the same semantics. Therefore, we consider whether incorporating VFMs into the pre-fine-tuning process could further enhance the CLIP’s feature correlations.

However, we observe that the direct distillation approach fails to achieve satisfactory results. Specifically, we adopt the typical region Vision-Language (V-L) alignment approach [15] as the baseline (referred to as self-distillation, as illustrated in Fig. 4(b)), while concurrently performing VFM distillation<sup>3</sup>. As presented in Tab. 1 (row 2), simultaneously performing VFM distillation and self-distillation leads to a decrease in region classification performance. We hypothesize that spatial correlation and V-L alignment have different optimization focuses, and optimizing them simultaneously within a single model results in trade-offs.

## 4. METHOD

Through the above analysis, we found that CLIP underperforms in dense perception tasks since its image tokens fail to effectively aggregate information from semantically related regions (i.e., “proxy token” effect). The observation of VFM’s attention maps inspires us to leverage VFM to improve CLIP’s dense features. Considering the optimization conflict between feature correlations and V-L alignment, we apply a decoupled feature enhancement strategy to CLIP.

In this section, we present DeCLIP, an unsupervised fine-tuning framework for adapting CLIP to dense perception tasks. We first explain how to decouple CLIP’s self-attention mechanism into “content” and “context” components (Sec. 4.1). Then, in Sec. 4.2, we illustrate how to enhance context features

<sup>2</sup>The final vision-language projection layer is omitted here for brevity.

<sup>3</sup>VFM distillation refers to aligning the feature self-correlations between CLIP’s  $\mathbf{X}_{\text{dense}}$  and those of the VFM.

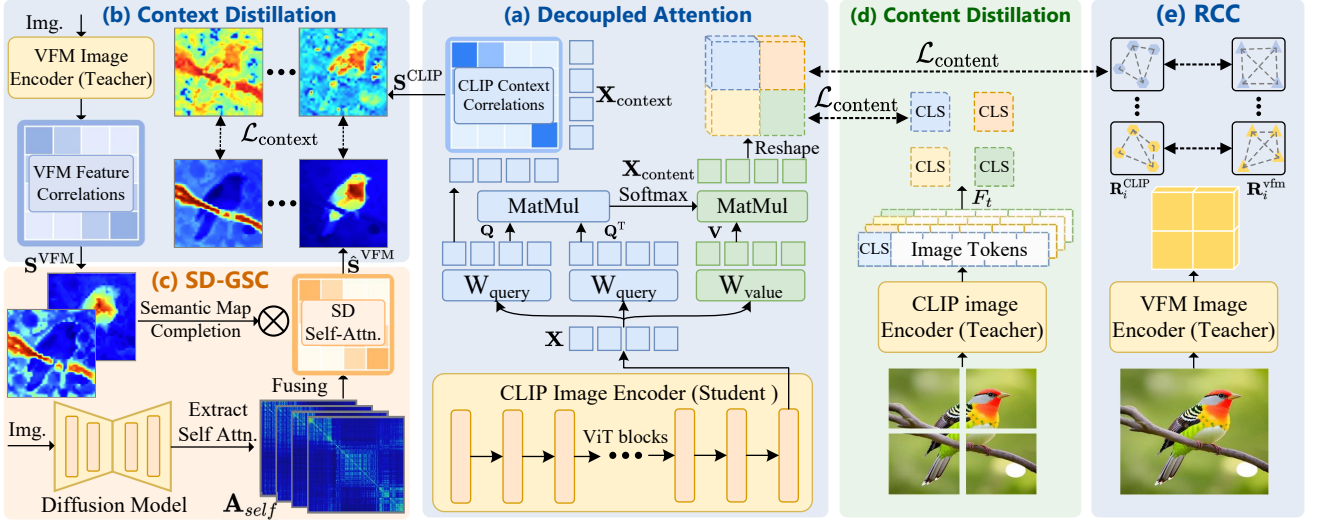


Fig. 5: **Illustration of the DeCLIP framework.** (a) **Decoupled Attention:** The final attention module of CLIP is decoupled into context features (to enhance spatial consistency) and content features (to enhance local vision-language alignment). (b) **Context Distillation:** Enhancing context features by leveraging semantic affinity maps from the VFM. (c) **SD-Guided Semantic Completion (SD-GSC):** The self-attention maps of SD are leveraged to enhance the semantic affinity map of VFMs and further optimize the distillation signals for the context features. (d) **Content Distillation:** Enhancing content features by aligning region representations with the corresponding [CLS] tokens. (e) **Region Correlation Constraint (RCC):** Using VFM’s region correlations to prevent the collapse of CLIP’s dense correlations during content distillation.

by distilling from VFM’s semantic affinity maps, and how to further refine these affinity maps using the self-attention maps of SD. Subsequently, we elaborate on how to enhance the content features using the [CLS] representation from CLIP and the region correlations from VFM.

#### 4.1 Decoupled Attention

The unsuccessful attempts to simultaneously perform self-distillation and VFM distillation on  $\mathbf{X}_{\text{dense}}$  (Tab. 1, row 2) prompt us to explore the feasibility of a decoupled distillation. In the following, we propose decoupling CLIP’s self-attention module to obtain “content” and “context” features, and separately optimize the local discriminability and spatial consistency abilities, as illustrated in Fig. 5(a).

**Rethinking the Self-Attention.** As described in Sec. 3.1, in CLIP’s last attention block, the  $\mathbf{V}$  features are weighted and summed under the guidance of the attention map ( $\text{Attn}_{qk}$ ) derived from  $\mathbf{Q}$  and  $\mathbf{K}$ , which define spatial or semantic correlations among image tokens. Studies [57]–[60] have shown that CLIP’s dense features  $\mathbf{X}_{\text{dense}}$  can be directly used for semantic segmentation by per-pixel classification, indicating that each pixel of  $\mathbf{X}_{\text{dense}}$  contains independent semantic information. Inspired by this, we regard  $\mathbf{Q}$  and  $\mathbf{K}$  as anchors for improving spatial consistency, and  $\mathbf{X}_{\text{dense}}$  as an anchor for enhancing local discriminability.

Additionally, recent training-free OVSS studies [57], [59] have further promoted us to decouple CLIP’s self-attention followed by distillation. They modify CLIP’s attention block from  $\text{Attn}_{qk}$  to  $\text{Attn}_{qq}$  and remove the residual connections, simplifying the optimization of local feature consistency by focusing on  $\mathbf{Q}$  alone. Based on our rethinking of CLIP’s

self-attention and inspired by these methods, we propose decoupling CLIP’s last attention block to obtain “content” and “context” features for distillation as follows:

$$\mathbf{X}_{\text{context}} = \text{Proj}_q(\mathbf{X}), \mathbf{V} = \text{Proj}_v(\mathbf{X}), \quad (4)$$

$$\mathbf{X}_{\text{content}} = \text{Proj}(\text{Attn}_{\text{context}} \cdot \mathbf{V}), \quad (5)$$

$$\text{Attn}_{\text{context}} = \text{SoftMax}(\mathbf{X}_{\text{context}} \mathbf{X}_{\text{context}}^\top / \sqrt{d}). \quad (6)$$

Specifically,  $\mathbf{V}$  is aggregated based on the attention map ( $\text{Attn}_{\text{context}}$ ) generated from  $\mathbf{X}_{\text{context}}$ .  $\mathbf{X}_{\text{context}}$  determines which image tokens are semantically or spatially related.  $\mathbf{X}_{\text{content}}$  carries the semantic information of each image token in the V-L space. By decoupling the features in this manner, we can apply different guidance constraints to  $\mathbf{X}_{\text{context}}$  and  $\mathbf{X}_{\text{content}}$  to obtain diverse feature representations in a unified architecture without interference. As observed in Sec. 3.2, VFM demonstrates a strong correlation among image tokens with the same semantics. Therefore, we leverage it as guidance for  $\mathbf{X}_{\text{context}}$  to enhance the spatial consistency of CLIP’s dense features. Meanwhile, we utilize CLIP’s [CLS] representation for sub-images [15] as guidance for  $\mathbf{X}_{\text{content}}$  to improve the local V-L alignment of CLIP’s dense features.

As shown in Tab. 1 (row 3), this decoupled optimization significantly enhances the local discriminability and spatial consistency of CLIP’s features, resulting in simultaneous improvements in both region classification accuracy and semantic segmentation performance.

#### 4.2 DeCLIP

The previous section presents a method for obtaining the decoupled “context” and “content” features from CLIP. In this section, we elaborate on how the decoupled features  $\mathbf{X}_{\text{content}}$



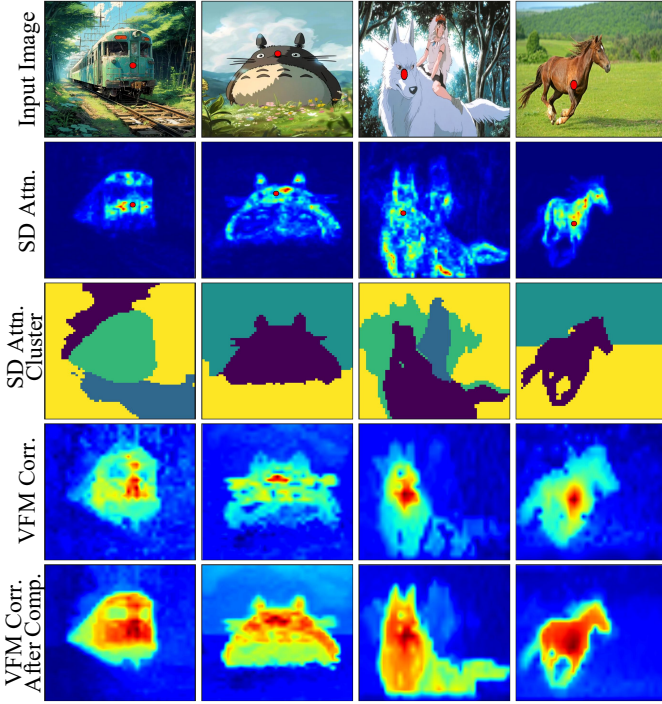


Fig. 6: **Visualization of VFM semantic affinity maps before and after semantic completion.** The cosine similarity and attention between the query token (red dot) and the remaining image tokens are visualized. SD attention maps are highly sensitive to high-frequency features, especially object contours (second row). K-means clustering of SD attention maps demonstrates notable object integrity (third row). Before completion (fourth row), the VFM semantic affinity map is blurred at boundaries and contains internal gaps. After completion (last row), the affinity map exhibits improved object integrity.

and  $\mathbf{X}_{\text{context}}$  learn from their respective teacher models to enhance CLIP’s performance on OV dense perception tasks.

**Context Feature Distillation.** As discussed in Sec. 3.2, VFMs do not exhibit CLIP’s “proxy” token issue and better correlate semantically related image tokens, which may be conducive to the fine-grained local perception. Therefore, we distill these correlations into CLIP’s  $\mathbf{X}_{\text{context}}$  features.

As illustrated in Fig. 5(b), given an input image  $\mathbf{I}$ , the VFM processes it and obtains feature representations  $\mathbf{X}_{\text{dense}}^{\text{VFM}} \in \mathbb{R}^{C \times HW}$ . Here,  $D$  represents the channel dimension of the VFM. Meanwhile, the student CLIP model takes the image  $\mathbf{I}$  as input and outputs the content feature  $\mathbf{X}_{\text{content}} \in \mathbb{R}^{C \times H \times W}$  and the context feature  $\mathbf{X}_{\text{context}} \in \mathbb{R}^{C \times HW}$ , as mentioned in Eq.(6). Here,  $C$  represents the dimension of the CLIP visual encoder. To ensure consistency in the number of image tokens after patch embedding, different input resolutions are typically used for the VFM and the student CLIP.

To facilitate the transfer of semantic affinities among VFM features to CLIP’s dense features, an intermediary is necessary to represent the correlation between pairs of image tokens. In

our method, cosine similarity is employed as follows<sup>4</sup>:

$$\mathbf{S}^{\text{VFM}} = \cos((\mathbf{X}_{\text{dense}}^{\text{VFM}})^{\top}, \mathbf{X}_{\text{dense}}^{\text{VFM}}) \quad (7)$$

where  $\mathbf{S}^{\text{VFM}} \in \mathbb{R}^{HW \times HW}$  denotes the similarity matrix of the entire VFM feature, where each entry  $\mathbf{S}_{ij}^{\text{VFM}}$  represents the cosine similarity between patch tokens  $\mathbf{x}_i$  and  $\mathbf{x}_j$ . Based on the analysis in Sec. 3.2, it is possible to improve CLIP dense features by leveraging the semantic affinity capability of VFM. A straightforward method involves aligning the correlations between  $\mathbf{S}^{\text{VFM}}$  and  $\mathbf{X}_{\text{context}}$  using either KL divergence or L2 loss. However, as shown in the fourth row of Fig. 6, VFM’s affinity map  $\mathbf{S}^{\text{VFM}}$  suffers from a lack of object integrity, exhibiting unclear boundaries and internal holes.

**SD-Guided Semantic Completion.** OV dense perception tasks require continuous and consistent predictions. However, the limited object integrity in VFM semantic affinity maps may lead to suboptimal distillation signals for context features. To address this limitation, we focus on another foundation model, the SD models [21], which are capable of generating high-quality images conditioned on textual descriptions.

We hypothesize that the self-attention modules [52], [53] in the SD model [3] effectively capture object boundaries and layout details [61], [62], which are crucial for generating high-resolution and realistic images. As illustrated in Fig. 6 (row 2), we visualize the  $8 \times$  downsampled self-attention maps of SD. They clearly delineate the main object layout and contour details within the image. The K-means clustering results further demonstrate the effectiveness of SD self-attention in capturing object integrity (row 3, Fig. 6). However, these maps are less effective than VFM’s semantic affinity maps in capturing semantic discrimination. As shown in Fig. 6 (column 3), SD’s attention incorrectly attends to the girl in the image (with the query token on the wolf), whereas the VFM’s semantic affinity map does not. The inferior results of directly distilling SD’s attention map (Tab. 9) further support this observation. On the other hand, this property complements VFM, whose semantic affinity maps are relatively accurate but lack object integrity. Therefore, we leverage SD’s self-attention maps to further enhance the distillation signals from VFM for context features.

Specifically, the same image  $\mathbf{I}$ , along with an empty text prompt, is fed into the SD model to extract the self-attention maps from the U-Net. The self-attention maps are denoted as  $\mathbf{A}_{\text{self}} \in \mathbb{R}^{L \times HW \times HW}$ , where  $L$  represents the total number of attention heads across all layers. Following [61], [63], matrix chain multiplication is employed to fuse attention maps across different layers and heads, as shown below:

$$\hat{\mathbf{A}}_{\text{self}} = \prod_{i=1}^L \mathbf{A}_{\text{self}}[i]. \quad (8)$$

Where  $\hat{\mathbf{A}}_{\text{self}} \in \mathbb{R}^{HW \times HW}$  represents the fused attention map. Subsequently, the fused attention map  $\hat{\mathbf{A}}_{\text{self}}$  is multiplied with the semantic affinity map  $\mathbf{S}^{\text{VFM}}$  generated by VFM to incorporate object boundary information. The results are presented in the last row of Fig. 6.

<sup>4</sup>For simplicity, we use  $\cos(\cdot, \cdot)$  to denote the computation of cosine similarity between two matrices.

$$\hat{\mathbf{S}}^{\text{VFM}} = \hat{\mathbf{A}}_{\text{self}} \times \mathbf{S}^{\text{VFM}}. \quad (9)$$

Subsequently, we use the KL divergence loss to align the similarity matrix  $\mathbf{S}^{\text{CLIP}} \in \mathbb{R}^{HW \times HW}$  produced from  $\mathbf{X}_{\text{context}}$  with the completed  $\hat{\mathbf{S}}^{\text{VFM}} \in \mathbb{R}^{HW \times HW}$ , as illustrated below:

$$\mathcal{L}_{\text{context}} = \frac{1}{HW} \sum_{i=1}^{HW} \text{KL} \left( \hat{\mathbf{S}}_{i,:}^{\text{VFM}}, \mathbf{S}_{i,:}^{\text{CLIP}} \right), \quad (10)$$

Notably, even with the introduction of the SD model, our DeCLIP fine-tuning framework still maintains efficacy and does not require any additional textual queries or annotations.

**Content Feature Distillation.** As shown in Fig. 5(d), the second teacher model in DeCLIP is itself, which is known as self-distillation [15], [44], [64], [65]. We employ image patching to align the region representations of the student model’s feature map  $\mathbf{X}_{\text{content}}$  with the corresponding image crop representations (i.e., [CLS] token) of the teacher model.

Specifically, the input image  $\mathbf{I}$  is initially partitioned into  $k$  sub-regions. Subsequently, these sub-regions are cropped from the original image, resulting in a set of sub-images  $S = \{\mathbf{I}'_1, \mathbf{I}'_2, \dots, \mathbf{I}'_k\}$ . Then, the student model applies RoI Align [66] to obtain pooled region features from  $\mathbf{X}_{\text{content}}$  using the cropping coordinates of  $S$ , resulting in a region feature set  $F_s = \{\mathbf{f}_1^s, \mathbf{f}_2^s, \dots, \mathbf{f}_k^s\}$ , where  $\mathbf{f}_i^s \in \mathbb{R}^{N^2 \times C}$ , and  $N$  denotes the size of each RoI region.

Meanwhile, the teacher model takes the sub-image set  $S$  as input and outputs a series of [CLS] tokens corresponding to the cropped sub-images, resulting in [CLS] token set  $F_t = \{\mathbf{f}_1^t, \mathbf{f}_2^t, \dots, \mathbf{f}_k^t\}$ , where  $\mathbf{f}_i^t \in \mathbb{R}^{C \times 1}$ . For each region feature  $\mathbf{f}_i^s$  generated by the student model, we compute a weighted summation according to its similarity with the teacher’s [CLS] token  $\mathbf{f}_i^t$  to obtain  $\bar{\mathbf{f}}_i^s$ , as defined below:

$$\bar{\mathbf{f}}_i^s = \text{softmax}(\cos(\mathbf{f}_i^s, \mathbf{f}_i^t))^\top \cdot \mathbf{f}_i^s \quad (11)$$

where  $\bar{\mathbf{f}}_i^s \in \mathbb{R}^{1 \times C}$ . We employ a cosine similarity loss to align the teacher’s [CLS] representations from  $F_t$  with the region features obtained by weighted summation from  $F_s$ , as follows:

$$\mathcal{L}_{\text{content}} = \frac{1}{k} \sum_{i=1}^k 1 - \cos(\bar{\mathbf{f}}_i^s, \mathbf{f}_i^t). \quad (12)$$

The intuition of this distillation branch is that the [CLS] token in CLIP acquires strong representational capabilities through contrastive learning on large-scale image-text pairs, as described in Sec. 3.1. Therefore, aligning the region features in CLIP, i.e.,  $F_s = \{\mathbf{f}_1^s, \mathbf{f}_2^s, \dots, \mathbf{f}_k^s\}$ , with the corresponding [CLS] representations, i.e.,  $F_t = \{\mathbf{f}_1^t, \mathbf{f}_2^t, \dots, \mathbf{f}_k^t\}$ , enhances the local discriminative capability of its dense features.

**Region Correlation Constraint.** As shown in the third column of Fig 7, we empirically find that directly aligning regional features and their corresponding [CLS] representations may further weaken the correlations of CLIP’s dense features. Therefore, we utilize an additional constraint term during the content distillation process to prevent the degradation of CLIP’s dense correlations by leveraging those of the VFM.

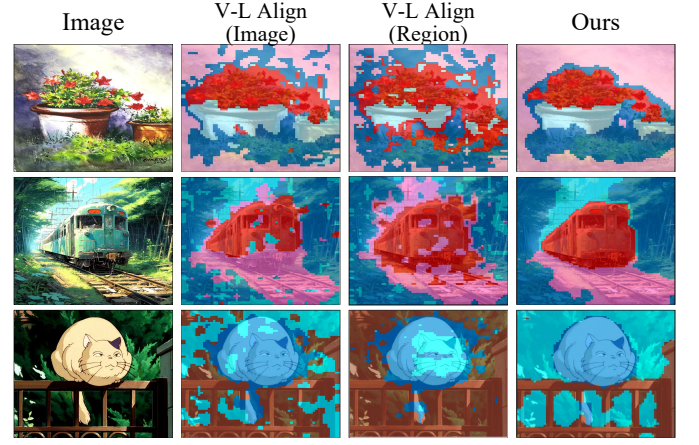


Fig. 7: **Comparison of feature semantic consistency before and after region-level fine-tuning.** “V-L align (Image)” refers to the vanilla CLIP, while “V-L align (Region)” denotes existing fine-tuning approaches [15], [16]. By performing K-means clustering on the cosine similarity maps of CLIP features, we observe that region-level fine-tuning may further weaken the pixel-level perception capability of CLIP.

Specifically, we first restore the spatial dimensions of the VFM features to obtain  $\mathbf{X}_{\text{dense}}^{\text{VFM}} \in \mathbb{R}^{C \times H \times W}$ . Then, we use RoI Align [66] with the cropping coordinates to extract the regional representations of VFM, resulting in  $F_{\text{vfm}} = \{\mathbf{f}_1^{\text{vfm}}, \mathbf{f}_2^{\text{vfm}}, \dots, \mathbf{f}_k^{\text{vfm}}\}$ , where  $\mathbf{f}_i^{\text{vfm}} \in \mathbb{R}^{N^2 \times D}$ . Subsequently, we employ the KL divergence to align the internal correspondences of regional features between CLIP and VFM [67]. The new content loss is defined as follows:

$$\mathcal{L}_{\text{content}} = \frac{1}{k} \sum_{i=1}^k 1 - \cos(\bar{\mathbf{f}}_i^s, \mathbf{f}_i^t) + \text{KL}(\mathbf{R}_i^{\text{vfm}}, \mathbf{R}_i^{\text{CLIP}}) \quad (13)$$

$$\mathbf{R}_i^{\text{vfm}} = \cos(\mathbf{f}_i^{\text{vfm}}, (\mathbf{f}_i^{\text{vfm}})^\top), \quad \mathbf{R}_i^{\text{CLIP}} = \cos(\mathbf{f}_i^s, (\mathbf{f}_i^s)^\top) \quad (14)$$

Finally, the entire distillation learning process of DeCLIP is summarized as follows:

$$\mathcal{L}_{\text{total}} = \mathcal{L}_{\text{content}} + \lambda \mathcal{L}_{\text{context}}. \quad (15)$$

## 5. EXPERIMENTS

### 5.1 Experiment Details

**Training Settings.** DeCLIP is trained on the training set of COCO2017 [68] using 8 GPUs, each with a batch size of 2, for 6 epochs (about 20 min/epoch). The AdamW [69] optimizer with a learning rate of  $1e-5$  and a weight decay of 0.1 is employed during the training process. Unless otherwise specified, we use EVA-CLIP [70] as the VLM baseline in our experiments and fine-tune all of its encoder layers by default. We did not apply any augmentation to the input images because such operations are found to degrade performance.

**Hyperparameter Settings.** By default, we perform context feature distillation for DeCLIP’s ViT-B and ViT-L using the DINOv2 [55] ViT-B and ViT-L models with registers [71]. We use input images with different resolutions for CLIP and VFM models to maintain a consistent number of tokens after



TABLE 2: **Quantitative results of OV 3D instance segmentation evaluated on the ScanNet200 dataset.** DeCLIP significantly enhances the performance of existing 3D instance segmentation methods and achieves the highest results.

Method	Setting	3D Proposal	AP	AP <sub>50</sub>	AP <sub>25</sub>	AP <sub>head</sub>	AP <sub>tail</sub>
ISBNNet [73]	Fully-sup	None	24.5	32.7	37.6	38.6	12.5
Mask3D [74]	Fully-sup	None	26.9	36.2	41.4	39.8	17.9
OpenScene [75] + DBScan [76]	Open-vocab	None	2.8	7.8	18.6	2.7	2.6
OpenScene [75] + Mask3D [74]	Open-vocab	Mask3D [74]	11.7	15.2	17.8	13.4	9.9
SAM3D [33]	Open-vocab	None	6.1	14.2	21.3	7.0	4.6
OVIR-3D [34]	Open-vocab	None	13.0	24.9	32.3	14.4	11.7
OpenIns3D [77]	Open-vocab	Mask3D [74]	8.8	10.3	14.4	16.0	4.2
OpenMask3D [37]	Open-vocab	Mask3D [74]	15.4	19.9	23.1	17.1	14.9
Open3DIS (2D) [36]	Open-vocab	None	18.2	26.1	31.4	18.9	19.2
Open3DIS (3D) [36]	Open-vocab	ISBNNet [73]	18.6	23.1	27.3	24.7	13.3
Open3DIS (2D+3D) [36]	Open-vocab	ISBNNet [73]	23.7	29.4	32.8	21.2	21.8
OpenMask3D + DeCLIP	Open-vocab	Mask3D [74]	18.3 (+2.9)	23.4 (+3.5)	26.8 (+3.7)	18.4 (+1.3)	18.9 (+4.0)
Open3DIS (2D+3D) + DeCLIP	Open-vocab	ISBNNet [73]	26.4 (+2.7)	32.8 (+3.4)	36.2 (+3.4)	28.2 (+7.0)	27.7 (+5.9)

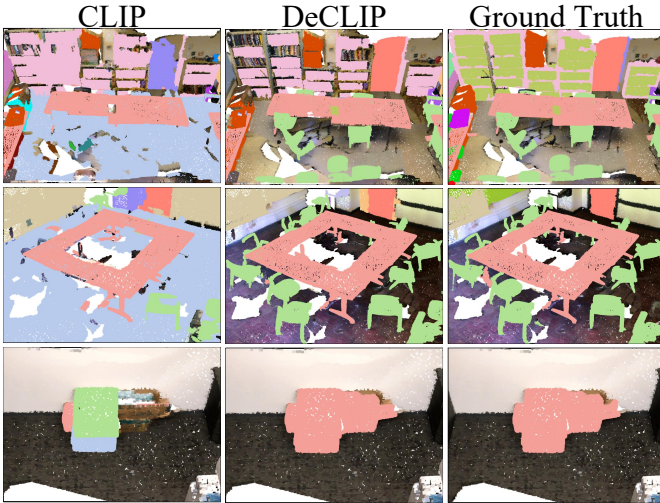


Fig. 8: Qualitative comparison of OV 3D instance segmentation results between CLIP and DeCLIP on the ScanNet200 [72] dataset. The baseline method is Open3DIS [36].

patch embedding, since CLIP uses a patch size of 16 while DINOv2 uses 14. For example, we set the input resolution for CLIP to 560 and for DINOv2 to 490, ensuring both models possess 1225 image tokens. Following [61], [63], we extract self-attention maps from the 45th time-step (out of 50 steps) of Stable Diffusion V2.1 [21] for the SD-guided semantic completion module. Following [15], for the content feature distillation branch, we partition the image into  $k$  blocks, where  $k = m \times n$  and  $m$  and  $n$  are randomly sampled from the range [1, 6]. The weight  $\lambda$  for context feature distillation is set to 0.25 by default. Distinct image normalization hyperparameters are set for the VFM, CLIP, and SD models, consistent with the settings applied during their respective pre-training.

## 5.2 Applications to OV Dense Perception Tasks

In this section, we conduct a comprehensive evaluation of the proposed DeCLIP method on multiple OV dense perception benchmarks to demonstrate its potential as a foundational model for such tasks. In terms of task types, our evalua-

tion encompasses OV detection, OV semantic segmentation (including training-free OV semantic segmentation), OV 3D instance segmentation, OV video instance segmentation, and OV 6D object pose estimation. In terms of data types, our evaluation covers 2D, 3D, and video data scenarios. We will present the performance improvements brought by DeCLIP to each of these tasks in the following content in turn.

**OV 3D Instance Segmentations.** In this task, we use OpenMask3D [37] and Open3DIS [36] as baselines to evaluate the effectiveness of DeCLIP in the 3D OV segmentation task. Apart from replacing the CLIP model in these two methods with DeCLIP, all other settings remain consistent with the original papers.

- **Dataset and Evaluation Metrics:** The dataset used for evaluation is ScanNet200 [72], a large-scale dataset with a long-tailed distribution, consisting of 1,201 training scenes and 312 validation scenes. We evaluate using the standard AP metrics at IoU thresholds of 0.5 (AP<sub>50</sub>) and 0.25 (AP<sub>25</sub>), as well as the mAP across IoU thresholds from 0.5 to 0.95 in increments of 0.05 (AP). Furthermore, we report the AP for specific category groups, including AP<sub>head</sub> and AP<sub>tail</sub>.
- **Results:** The quantitative evaluation of ScanNet200 is summarized in Tab. 2. By replacing the vanilla CLIP with our proposed DeCLIP, the performance of both OpenMask3D (14.9 vs. 18.9 on the AP<sub>tail</sub> metric) and Open3DIS (21.8 vs. 27.7 on the AP<sub>tail</sub> metric) is significantly improved. Moreover, our DeCLIP surpasses existing 3D OV instance segmentation methods. Fig. 8 presents a qualitative comparison between CLIP and DeCLIP on ScanNet200.

**OV Video Instance Segmentation.** We employ CLIP-VIS [38] as the baseline to evaluate the effectiveness of DeCLIP in the video dense perception task. Only the backbone network of CLIP-VIS is replaced with DeCLIP, which remains frozen during training, while all other settings are kept consistent with the original paper. Additionally, since CLIP-VIS extracts multi-scale features from CLIP, to remain consistent with the original paper, we extract features from layers [3, 5, 7, 11] of DeCLIP-B/16 and layers [6, 10, 14, 23] of DeCLIP-L/14, and obtain multi-scale features through downsampling and transposed convolution.

TABLE 3: **Quantitative results on the OV video instance segmentation task.** ‘/’ indicates that training and evaluation are conducted on the same dataset, representing the reference results of conventional closed-set video instance segmentation. The combination of CLIP-VIS and DeCLIP achieves new state-of-the-art results on this task.

Method	Training Data	Backbone	LV-VIS val		LV-VIS test		OVIS	YTVIS19	YTVIS21	BURST	
			AP	AP <sub>N</sub>	AP	AP <sub>N</sub>	AP	AP	AP	AP	AP <sub>N</sub>
Classical video instance segmentation											
MaskTrack R-CNN [78]	/	R50	–	–	–	–	10.8	30.3	28.6	–	–
Mask2Former [4]	/	R50	–	–	–	–	17.3	46.4	40.6	–	–
IDOL [79]	/	R50	–	–	–	–	30.2	49.5	43.9	–	–
OV video instance segmentation											
Detic [28]+SORT [80]	LVIS	SwinB	12.8	6.6	9.4	4.7	11.7	23.8	21.6	2.5	1.0
Detic [28]+OWTB [81]	LVIS	SwinB	14.5	11.8	13.6	5.5	30.0	9.7	11.4	3.9	2.4
Detic [28]+XMem [82]	LVIS	SwinB	16.3	10.6	13.1	7.7	–	–	–	–	–
OV2Seg [83]	LVIS	SwinB	21.1	16.3	16.4	11.5	17.5	37.6	33.9	4.9	3.0
OVFormer [40]	LVIS	SwinB+ViT-B	–	–	–	–	21.3	44.3	37.6	–	–
CLIP-VIS [38]	LVIS	ConvNeXt-B	32.2	40.2	25.3	30.6	18.5	42.1	37.9	8.3	12.7
CLIP-VIS+DeCLIP	LVIS	ViT-B/16	34.8	44.3	28.4	34.0	22.2	50.6	43.3	8.9	15.7
CLIP-VIS+DeCLIP	LVIS	ViT-L/14	<b>37.7</b>	<b>45.9</b>	<b>30.9</b>	<b>36.9</b>	<b>29.3</b>	<b>54.8</b>	<b>49.1</b>	<b>10.1</b>	<b>16</b>



Fig. 9: Qualitative comparison of OV video instance segmentation results between CLIP and DeCLIP on the YTVIS21 [84] dataset. The baseline method is CLIP-VIS [38].

- **Dataset and Evaluation Metrics:** We train CLIP-VIS on the training set of the LVIS [85]. The evaluation datasets include both the validation and test sets of the LV-VIS dataset [83], as well as the validation sets of several other video instance segmentation benchmarks: OVIS [86], YTVIS2019/2021 [84], and BURST [87]. We use the standard mean AP within the IoU range of 0.5 to 0.95 as the evaluation metric (AP). Additionally, OV tasks primarily focus on the performance of unseen category objects, so we separately report the AP metric for novel categories (AP<sub>N</sub>).
- **Results:** The quantitative results of applying DeCLIP to video instance segmentation tasks are summarized in Table 3. DeCLIP leads to significant performance improvement across all the evaluation datasets. Fig. 9 presents a qualitative comparison between DeCLIP and vanilla CLIP-VIS (using CLIP as the backbone) on the YTVIS21 dataset.

**OV Object 6D Pose Estimation.** Oryon [35] originally introduced this task, which aims to infer the position and orientation of arbitrary objects in three-dimensional space from images or point clouds based on language descriptions. We use Oryon as the baseline for this task. For all experiments,

we follow the default training and inference settings of the vanilla Oryon model, with the only modification being the replacement of the image encoder with DeCLIP.

- **Dataset and Evaluation Metrics:** Following Oryon’s open-vocabulary setting [35], we train our model on the ShapeNet6D [88], [89] dataset and evaluate it on the REAL275 [90] and Toyota-Light (TOYL) [91] datasets. Similar to Oryon, we evaluate the pose estimation results using the metrics proposed by the BOP benchmark [92], including AR, VSD, MSSD, and MSPD. For the specific meanings of these metrics, please refer to [92]. Additionally, the Oryon model includes a decoding head for predicting object masks. Therefore, we also report the improvement in the object mask prediction quality metric (mIoU) after replacing the backbone network with DeCLIP.
- **Quantitative Results:** As shown in Tab. 5, for the most important metric AR (Average Recall, average of VSD, MSSD, and MSPD), DeCLIP achieves performance improvements of 5.4 on REAL275 and 2.3 on TOYL compared to Oryon. Additionally, DeCLIP outperforms Oryon in object mask prediction quality, achieving improvements



TABLE 4: **Comparison with state-of-the-art OV object detection methods.** Caption supervision indicates learning from extra image-text pairs, while CLIP supervision refers to transferring knowledge from CLIP.  $\dagger$ : DETR-based detectors [94].

Method	Supervision	Backbone	AP <sub>Novel</sub> <sub>50</sub>
<b>OV-COCO</b>			
ViLD [18]	CLIP	RN50	27.6
Detic [28]	Caption	RN50	27.8
OV-DETR $\dagger$ [29]	CLIP	RN50	29.4
BARON-KD [9]	CLIP	RN50	34.0
SAS-Det [27]	CLIP	RN50	37.4
OV-DQUO $\dagger$ [17]	CLIP	RN50	39.2
RegionCLIP [16]	Captions	RN50x4	39.3
CORA $\dagger$ [10]	CLIP	RN50x4	41.7
OV-DQUO $\dagger$ [17]	CLIP	RN50x4	45.6
RO-ViT [95]	CLIP	ViT-L/16	33.0
CFM-ViT [96]	CLIP	ViT-L/16	34.1
F-ViT+CLIPSelf [15]	CLIP	ViT-B/16	37.6
F-ViT+CLIPSelf [15]	CLIP	ViT-L/14	44.3
F-ViT [15]+DeCLIP	CLIP	ViT-B/16	43.3 (+5.7)
F-ViT [15]+DeCLIP	CLIP	ViT-L/14	50.2 (+5.9)
OV-DQUO+DeCLIP $\dagger$	CLIP	ViT-B/16	47.3 (+8.1)
OV-DQUO+DeCLIP $\dagger$	CLIP	ViT-L/14	49.5 (+3.9)

Method	Supervision	Backbone	mAP <sub>r</sub>
<b>OV-LVIS</b>			
ViLD [18]	CLIP	RN50	16.3
OV-DETR $\dagger$ [29]	CLIP	RN50	17.4
BARON-KD [9]	CLIP	RN50	22.6
RegionCLIP [16]	Caption	RN50x4	22.0
OV-SAM [46]	CLIP	RN50x16	24.0
CORA $\dagger$ [10]	Caption	RN50x4	28.1
F-VLM [19]	CLIP	RN50x64	32.8
CLIPSelf [15]	CLIP	ViT-B/16	25.3
OV-DQUO $\dagger$ [17]	CLIP	ViT-B/16	29.7
Detic [28]	Caption	Swin-B	33.8
RO-ViT [95]	CLIP	ViT-H/16	34.1
CLIPSelf [15]	CLIP	ViT-L/14	34.9
OV-DQUO $\dagger$ [17]	CLIP	ViT-L/14	39.3
F-ViT [15]+DeCLIP	CLIP	ViT-B/16	27.1 (+1.8)
F-ViT [15]+DeCLIP	CLIP	ViT-L/14	37.8 (+2.9)
OV-DQUO $\dagger$ +DeCLIP	CLIP	ViT-B/16	31.5 (+1.8)
OV-DQUO $\dagger$ +DeCLIP	CLIP	ViT-L/14	41.5 (+2.2)

TABLE 5: **Results on OV object 6D pose estimation.**  $\dagger$  denotes “oracle” performance using GT object masks for pose estimation. \* indicates our ViT-B results based on the official code, as Oryon uses the ViT-L version of CLIP by default.

Method	Backbone	Dataset	AR $\uparrow$	VSD $\uparrow$	MSSD $\uparrow$	MSPD $\uparrow$	mIoU $\uparrow$
Oryon $\dagger$	ViT-L/14	REAL275	46.5	32.1	50.9	56.7	100.0
Oryon*	ViT-B/16		28.8	18.9	32.4	35.1	57.4
Oryon	ViT-L/14		32.2	23.6	36.6	36.4	66.5
Oryon+DeCLIP	ViT-B/16		33.7	23.2	37.6	40.2	65.1
Oryon+DeCLIP	ViT-L/14		37.6	27.5	42.2	43.2	72.2
$\Delta$ Score	ViT-B/16	REAL275	(+4.9)	(+4.3)	(+5.2)	(+5.1)	(+7.7)
$\Delta$ Score	ViT-L/14	REAL275	(+5.4)	(+3.9)	(+5.6)	(+6.8)	(+5.7)
Oryon $\dagger$	ViT-L/14	TOYL	34.1	13.9	42.9	45.5	100.0
Oryon*	ViT-B/16		29.8	11.1	38.0	40.1	64.3
Oryon	ViT-L/14		30.3	12.1	37.5	41.4	68.1
Oryon+DeCLIP	ViT-B/16		31.9	11.8	40.3	43.5	71.4
Oryon+DeCLIP	ViT-L/14		32.6	12.7	41.2	43.8	68.7
$\Delta$ Score	ViT-B/16	TOYL	(+2.1)	(+0.7)	(+2.3)	(+3.4)	(+7.1)
$\Delta$ Score	ViT-L/14	TOYL	(+2.3)	(+0.6)	(+3.7)	(+2.4)	(+0.6)

of 5.7 on the REAL275 dataset and 0.6 on the TOYL dataset. Notably, Oryon utilizes a dual-encoder architecture (CLIP [12] and Swin Transformer [93]), with the Swin Transformer compensating for CLIP’s limitations in local representation. However, replacing CLIP with DeCLIP in Oryon still leads to a significant improvement in OV pose estimation performance. This further demonstrates the superiority of DeCLIP, which exhibits pixel-level vision-language alignment capabilities.

- **Qualitative Results:** as shown in Fig. 10, for the “brown open laptop” object in the REAL275 dataset, both Oryon (CLIP) and Oryon (DeCLIP) are able to estimate the object pose, but DeCLIP demonstrates greater precision in terms of detail. In contrast, for the “orange can” object in TOYL (under varying illumination conditions), CLIP fails in pose estimation, whereas DeCLIP still exhibits strong robustness.

**OV Object Detection.** In this task, DeCLIP is evaluated using two baseline models: F-ViT [15] and OV-DQUO [17]. F-ViT is based on the traditional Faster R-CNN [1] architecture, while

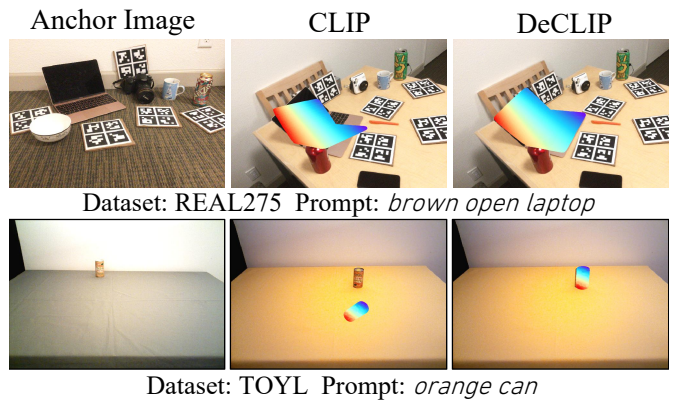


Fig. 10: Qualitative comparison of OV pose estimation results between CLIP and DeCLIP on REAL275 [90] and TOYL [91]. Following Oryon [35], we color the object model by mapping its 3D coordinates to the RGB space for visualization.

OV-DQUO adopts the modern Detection Transformer [94]. We replace only the backbone networks of F-ViT and OV-DQUO with DeCLIP, while keeping all other settings consistent with those in the original papers.

- **Dataset and Evaluation Metrics:** Following established settings [15], [17], we evaluate our model on the OV-COCO [68] and OV-LVIS [85] datasets. For the OV-COCO dataset, the mAP at an IoU threshold of 0.5 for novel categories ( $AP_{Novel}^{50}$ ) is adopted as the evaluation metric. For the OV-LVIS dataset, the mAP on rare categories at IoU thresholds ranging from 0.5 to 0.95 is adopted as the evaluation metric ( $mAP_r$ ).
- **Results:** Tab. 4 presents DeCLIP’s performance on OV-COCO and OV-LVIS benchmarks. On OV-COCO, DeCLIP improves the F-ViT [15] baseline by 5.7 and 5.9 mAP, and the OV-DQUO [17] baseline by 8.1 and 3.9 mAP on novel categories. On OV-LVIS, it achieves gains of 1.8 and 2.9

TABLE 6: Results on OV semantic segmentation. <sup>†</sup> indicates results re-experimented by CAT-Seg [11].

Method	Backbone	Training Set	ADE847	Context459	ADE150	Context59	VOC20	VOC21
ZegFormer <sup>†</sup> [97]	ViT-B/16	COCO-Stuff	5.6	10.4	18.0	45.5	89.5	65.5
ZSseg [98]	ViT-B/16	COCO-Stuff	7.0	-	20.5	47.7	88.4	-
OVSeg [20]	ViT-L/14	COCO-Stuff	9.0	12.4	29.6	55.7	94.5	-
SAN [99]	ViT-L/14	COCO-Stuff	13.7	17.1	33.3	60.2	95.5	-
ODISE [100]	ViT-L/14	COCO-Panoptic	11.1	14.5	29.9	57.3	-	84.6
MAFT [42]	ConvNeXt-L	COCO-Stuff	13.1	17.0	34.4	57.5	93.0	-
FC-CLIP [101]	ConvNeXt-L	COCO-Panoptic	14.8	18.2	34.1	58.4	95.4	81.8
FrozenSeg [47]	ConvNeXt-L	COCO-Panoptic	14.8	19.7	34.4	-	-	82.5
CAT-Seg [11]	ViT-B/16	COCO-Stuff	12.0	19.0	31.8	57.5	94.6	77.3
CAT-Seg [11]	ViT-L/14	COCO-Stuff	16.0	23.8	37.9	63.3	97.0	82.5
CAT-Seg+DeCLIP	ViT-B/16	COCO-Stuff	15.3 (+3.3)	21.4 (+2.4)	36.3 (+4.5)	60.6 (+3.1)	96.6 (+2.0)	81.3 (+4.0)
CAT-Seg+DeCLIP	ViT-L/14	COCO-Stuff	17.6 (+1.6)	25.9 (+2.1)	40.7 (+2.8)	63.9 (+0.6)	97.7 (+0.7)	83.9 (+1.4)

TABLE 7: Comparison with state-of-the-art training-free OV semantic segmentation methods.

Method	With a background category			Without background category					Avg.
	VOC21	Context60	COCO-Object	VOC20	CityScape	Context59	ADE	COCO-Stuff	
CLIP [12]	18.8	9.9	8.1	49.4	6.5	11.1	3.1	5.7	14.1
MaskCLIP [102]	43.4	23.2	20.6	74.9	24.9	26.4	11.9	16.7	30.3
GroupViT [25]	52.3	18.7	27.5	79.7	18.5	23.4	10.4	15.3	30.7
ReCo [103]	25.1	19.9	15.7	57.7	21.6	22.3	11.2	14.8	23.5
TCL [104]	51.2	24.3	30.4	77.5	23.5	30.3	14.9	19.6	33.9
SCLIP [57]	59.1	30.4	30.5	80.4	32.2	34.2	16.1	22.4	38.2
ClearCLIP [59]	51.8	32.6	33.0	80.9	30.0	35.9	16.7	23.9	38.1
NACLIP [105]	58.9	32.2	33.2	79.7	35.5	35.2	17.4	23.3	39.4
CLIPDINOiser [60]	62.1	32.4	34.8	80.9	31.7	35.9	20.0	24.6	40.3
ResCLIP [106]	61.1	33.5	35.0	<b>86.0</b>	35.9	36.8	18.0	24.7	41.4
ProxyCLIP [107]	61.3	35.3	37.5	80.3	<b>38.1</b>	39.1	20.2	26.5	42.3
DeCLIP (Ours)	<b>64.1</b>	<b>37.9</b>	<b>38.7</b>	<u>85.3</u>	<u>35.7</u>	<b>41.6</b>	<b>23.1</b>	<b>26.8</b>	<b>44.1</b>

mAP with F-ViT, as well as 1.8 and 2.2 mAP with OV-DQUO on rare classes.

**OV Semantic Segmentation.** In this task, we integrate DeCLIP into the CAT-Seg [11] baseline. For all experiments, we follow the default training and inference settings of vanilla CAT-Seg, with the only modification being the replacement of the image encoder with DeCLIP.

- **Dataset and Evaluation Metrics:** We train models on the COCO-Stuff dataset [108] following the original CAT-Seg [11] method, and evaluate them on the ADE20K [109], PASCAL VOC [110], and PASCAL-Context [111] datasets. The ADE20K, PASCAL-Context, and PASCAL VOC datasets each contain two sets of categories: A-150 (150 classes) and A-847 (847 classes) [112] for ADE20K, PC-59 (59 classes) and PC-459 (459 classes) for PASCAL-Context, and PAS-20 (20 object classes) and PAS-21 (20 classes plus background) for PASCAL VOC. We use mIoU as the evaluation metric for all experiments.
- **Results:** Tab. 6 presents the performance of the CAT-Seg [11] model with DeCLIP as the backbone on various OV semantic segmentation benchmarks. The results show that DeCLIP significantly enhances segmentation performance on all datasets. Notably, even with the ViT-B/16 version of DeCLIP, CAT-Seg nearly surpasses all existing SOTA methods that utilize substantially larger encoders like ConvNeXt-L [50]. When employing the ViT-L/14 version

of DeCLIP, the model achieves new SOTA results in OV semantic segmentation tasks.

**Training-Free OV Semantic Segmentation.** Unlike the OV semantic segmentation task, which requires training task-specific segmentation components using the base-category dataset, this task directly leverages CLIP’s dense feature map  $\mathbf{X}_{\text{dense}}$  for OV semantic segmentation. Following existing methods [57]–[59], we directly compute the cosine similarity between each pixel in the DeCLIP feature map and all category texts to achieve zero-shot semantic segmentation. For all datasets, we generate textual descriptions by utilizing the standard ImageNet prompts [12] in conjunction with their respective class names. No post-processing steps are applied. The low-resolution prediction result is up-sampled to the original resolution to obtain the final segmentation map.

- **Dataset and Evaluation Metrics:** The evaluation of this task does not require training and thus does not include a training set. The validation set comprises six widely used semantic segmentation benchmark datasets: PASCAL VOC 2012 [110], PASCAL Context [111], Cityscapes [113], ADE20K [109], COCO Stuff [68], and COCO Object [108]. For datasets that include a background category, we denote them as VOC21 and Context60, while those without a background category are denoted as VOC20 and Context59. We employ mIoU as the evaluation metric for these benchmarks.



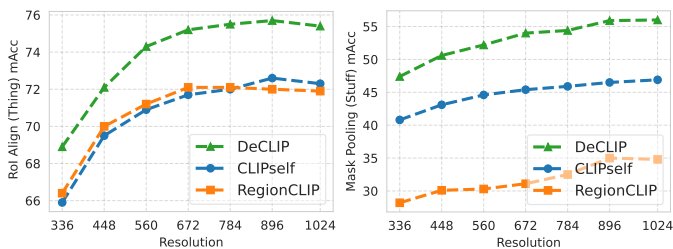


Fig. 11: Comparisons between DeCLIP and existing regional V-L alignment methods [15], [16] for OV region recognition performance on the COCO panoptic dataset. DeCLIP consistently outperforms existing methods at various resolutions.

TABLE 8: Ablation studies on the contributions of individual modules in DeCLIP for OV dense perception tasks. Performance is evaluated on OV detection (mAP) for novel categories on OV-COCO, as well as OV semantic segmentation (mIoU) on PASCAL VOC and COCO-Obj.

Content Distill.	Context Distill.	RCC	SD-GSC	OV-COCO	VOC21	COCO-Obj	Avg.
				17.5	43.4	20.6	27.2
✓				37.6	42.3	23.2	34.4
	✓			37.4	59.7	36.4	44.5
✓	✓			41.1	59.9	36.5	45.8
✓	✓	✓		42.5	60.5	36.9	46.6
✓	✓		✓	41.9	63.7	38.5	48.0
✓	✓	✓	✓	<b>43.3</b>	<b>64.1</b>	<b>38.7</b>	<b>48.7</b>

- **Results:** As shown in Tab. 7, DeCLIP outperforms all existing methods in terms of average mIoU across eight benchmarks, achieving an average mIoU of 44.1. This result highlights the effectiveness of our approach in enhancing the discriminability and spatial consistency of VLM features.

**OV Region Classification.** Following existing methods [15], [16], [114], we use the dataset annotations (boxes and masks) to extract region features from the feature map output by DeCLIP (using RoI Align [66] or Mask Pooling). Then, we compute the cosine similarity between these features and all text categories to achieve zero-shot region classification.

- **Dataset and Evaluation Metrics:** The evaluation of this task does not require training and thus does not include a training set. We employ Top-1 mean accuracy (mAcc) as the metric to evaluate the performance of models in classifying boxes and masks annotated in the COCO Panoptic [115].
- **Results:** As illustrated in Fig. 11, the Top-1 mAcc results indicate that DeCLIP consistently outperforms existing methods in region recognition across all resolutions.

### 5.3 Ablation Study

In this section, we conduct ablation studies to assess the effectiveness of the proposed method on OV dense perception tasks. For brevity, we report results on two typical dense perception tasks: OV object detection performance ( $AP_{50}^{Novel}$ ) on OV-COCO [68], and training-free OV semantic segmentation performance (mIoU) on PASCAL VOC [110] and COCO-obj [108]. We also report their average score (Avg).

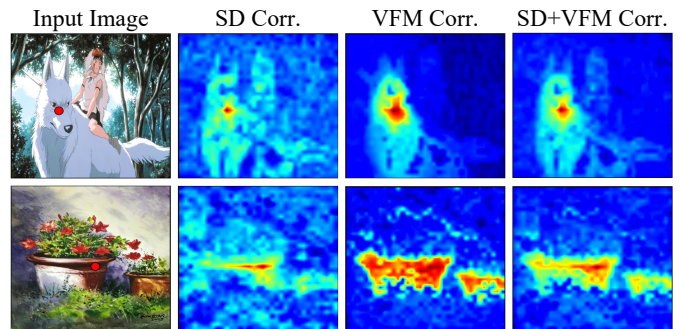


Fig. 12: Comparison of semantic affinity maps between SD and VFM features. Both SD features and the channel concatenation of SD and VFM features exhibit lower semantic affinity capability than using VFM features alone.

TABLE 9: Ablation Study on the collaboration strategies between VFM and SD. “Concat” combines VFM and SD features along the channel dimension. \* represents the weighted feature concatenation strategy. “DirectAlign” refers to the direct distillation of SD self-attention maps.

Method	VOC20	Context59	CityScene	ADE	COCO-Stf
Concat	75.2	30.6	24.4	19.2	19.9
Concat*	84.4	39.1	33.7	21.7	25.1
DirectAlign	79.6	32.0	28.5	18.0	21.3
SD-GSC	<b>85.3</b>	<b>41.6</b>	<b>35.7</b>	<b>23.1</b>	<b>26.8</b>

**Module Ablation.** We first assess the contributions of individual modules in DeCLIP through ablation experiments. Tab. 8 presents the incremental performance improvements obtained by successively incorporating Content Distillation, Context Distillation, Region Correlation Constraint (RCC), and SD-Guided Semantic Completion (SD-GSC).

Since CLIP features lack dense perception capabilities, we adopt MaskCLIP [102] as the baseline (Tab. 8, first row). As shown in Tab. 8, content distillation substantially improves detection performance on OV-COCO (from 17.5 to 37.6), but provides minimal benefit for segmentation tasks. In contrast, context distillation enhances both detection and segmentation performance, increasing the average score from 27.2 to 44.5. Combining content and context distillation yields additional gains in detection, achieving 41.1 on OV-COCO. Introducing RCC as a constraint for content distillation leads to a slight overall improvement in both detection and segmentation, with an average increase of 0.9. SD-GSC further boosts the performance of both tasks, resulting in a notable average increase of 2.3. Finally, the joint application of RCC and SD-GSC raises the average score to 48.7, achieving an overall gain of 3.0.

**Collaboration Strategies Between VFM and SD.** We systematically compare different cooperation strategies between VFM and SD models in the DeCLIP distillation framework. Specifically, we evaluate SD-GSC (used in the main text), feature concatenation [117], and direct distillation from SD’s self-attention maps, as shown in Tab. 9. The results indicate that SD-GSC achieves the best performance. Even when we carefully adjust the weights during feature concatenation (row 2, Tab. 9), the performance still remains unsatisfactory. Direct

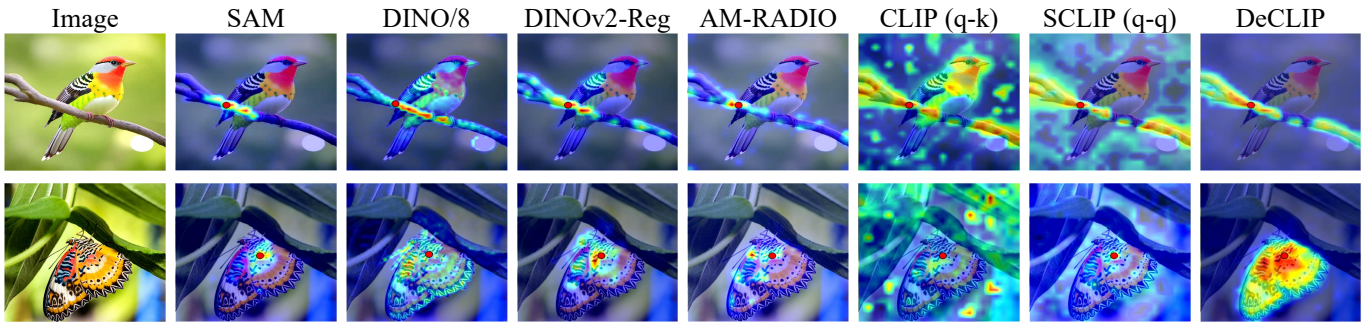


Fig. 13: **Qualitative comparisons of attention maps between existing methods and DeCLIP.** The comparison methods include: SAM [48], [56], trained on large-scale mask annotations; DINO [54] and DINOv2 [55] with registers [71], trained using a self-supervised approach; AM-RADIO [116], utilizing multi-teacher distillation from CLIP, SAM, and DINOv2 models; and SCLIP [57], incorporating correlative self-attention mechanisms. The query image token is marked in red.

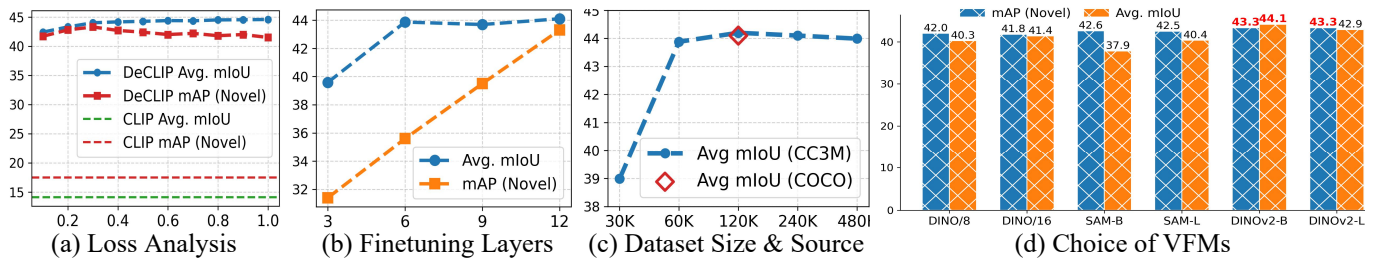


Fig. 14: **Ablation studies of DeCLIP method.** (a), (b), (c), and (d) denote the weight of the context loss, the number of fine-tuned layers in CLIP, the domain and scale of the distillation dataset, and the impact of VFM selection on OV dense perception performance (detection and segmentation), respectively. The segmentation results are averaged over multiple datasets. All experiments are performed using the ViT-B version of DeCLIP.

TABLE 10: Sanity check results of CAT-Seg with different backbones (CLIP, EVA-CLIP, and DeCLIP) to eliminate potential bias that may be introduced by EVA-CLIP.

Method	Backbone	ADE847	Context459	ADE150	Context59	VOC20	VOC21
CAT-Seg+CLIP	ViT-B/16	12.0	19.0	31.8	57.5	94.6	77.3
CAT-Seg+CLIP	ViT-L/14	16.0	23.8	37.9	63.3	97.0	82.5
CAT-Seg+EVA-CLIP	ViT-B/16	11.9	17.6	30.4	52.3	94.2	74.2
CAT-Seg+EVA-CLIP	ViT-L/14	14.2	21.3	34.8	56.2	95.8	80.1
CAT-Seg+DeCLIP	ViT-B/16	15.3	21.4	36.3	60.6	96.6	81.3
CAT-Seg+DeCLIP	ViT-L/14	17.6	25.9	40.7	63.9	97.7	83.9

TABLE 11: Sanity check experiments on training-free OV semantic segmentation to eliminate potential bias that may be introduced by EVA-CLIP.

Method	VOC21	Context60	COCO-Obj	CityScape	ADE	COCO-Stf
CLIP [12]	18.8	9.9	8.1	6.5	3.1	5.7
EVA-CLIP [70]	23.4	12.8	15.3	12.8	7.7	9.7
ClearCLIP [59]	51.8	32.6	33.0	30.0	16.7	23.9
EVA-ClearCLIP	47.0	29.7	30.2	26.3	16.7	20.4
DeCLIP	64.1	37.9	38.7	35.7	23.1	26.8

distillation with SD self-attention maps also underperforms compared to SD-GSC. We attribute this to the weaker semantic affinity of SD relative to VFM, as shown in Fig. 12.

**Sensitivity Analysis of  $\lambda$ .** We perform an ablation study to examine the relationship between the hyperparameter  $\lambda$  and dense perception performance, as shown in Fig. 14(a). Experimental results demonstrate that our method exhibits strong robustness, and the dense perception performance of DeCLIP does not fluctuate drastically with changes in  $\lambda$ . Furthermore, the results indicate that  $\lambda = 0.25$  strikes a good balance between OV detection and segmentation.

**Number of Fine-Tuning Layers.** We examine the relationship between the number of fine-tuning attention blocks and dense perception performance in Fig. 14(b). We observe that as the number of fine-tuning layers increases, the performance of OV detection and segmentation continuously improves, reaching its peak at 12 layers. Therefore, we chose to fine-tune all attention blocks in the implementation of DeCLIP.

**Sensitivity to Dataset Size and Source.** DeCLIP adopts the widely used COCO [68] dataset with 118k images as the default for distillation, following mainstream approaches [15], [16], [114]. This ensures fair comparisons and consistent experimental settings with existing methods. Additionally, we explore DeCLIP’s sensitivity to both the source and size of the distillation dataset. Specifically, we utilize the CC3M [118] dataset to examine how data size and source affect DeCLIP’s performance. CC3M is a dataset widely utilized for CLIP training in the literature, and its source differs from COCO. As shown in Fig. 14(c), DeCLIP is robust to these changes.

**Sensitivity to VFM Type and Size.** We further investigate the effect of different VFM choices on OV dense perception performance. This experiment covers various types of VFMs, such as SAM [48], [56], DINO [54], and DINOv2 [55], as well as different scale versions of the same type of VFM, such as ViT-B and ViT-L. As shown in Fig. 14(d), different VFMs and their size configurations have minimal



TABLE 12: Ablation studies on different VLM baselines. † indicates re-implementation based on the official code.

VLM Model	VOC21	Context60	COCO-Obj	CityScape	ADE	COCO-Stf
OpenAI-CLIP [12]	18.8	9.9	8.1	6.5	3.1	5.7
ClearCLIP [59]	51.8	32.6	33.0	30.0	16.7	23.9
DeCLIP	64.9	36.3	39.1	35.5	19.8	24.6
EVA-CLIP [70]	23.4	12.8	15.3	12.8	7.7	9.7
EVA-ClearCLIP† [59]	47.0	29.7	30.2	26.3	16.7	20.4
DeCLIP	64.1	37.9	38.7	35.7	23.1	26.8

impact on OV object detection performance. Among them, DINOv2 achieves the best results, followed by SAM and then DINO. In contrast, VFM selection significantly affects semantic segmentation tasks that require finer perceptual granularity. DINOv2-B achieves the highest performance in OV semantic segmentation, followed by DINOv2-L, the DINO series, and the SAM series. This can be attributed to the stronger semantic correspondence capability of DINOv2. Overall, DINOv2-B provides the best comprehensive performance. Fig. 13 presents the qualitative comparison of attention maps among SAM [48], DINO [54], DINOv2 [55] (with registers [71]), AM-RADIO<sup>5</sup> [116], CLIP [12], SCLIP [57], and DeCLIP. Experiments show that DeCLIP more effectively focuses on regions spatially or semantically associated with the query image token.

**Sanity Checks.** We conduct sanity checks to verify whether the performance improvement of DeCLIP in dense prediction stems from using EVA-CLIP. First, we use vanilla EVA-CLIP as the backbone in CAT-Seg [11] and compare its performance with DeCLIP on the OV semantic segmentation task (Tab. 10). Next, we re-implement ClearCLIP [59] with EVA-CLIP (termed EVA-ClearCLIP) and compare EVA-CLIP, EVA-ClearCLIP, and DeCLIP in the training-free OV semantic segmentation task (Tab. 11). Experimental results demonstrate that EVA-CLIP did not introduce any observable biases.

**Sensitivity to VLM Baseline.** DeCLIP adopts EVA-CLIP as the default VLM baseline to ensure fair comparison with existing methods [15]. To further assess its generalization, we evaluate DeCLIP on different VLMs. As shown in Tab. 12, DeCLIP maintains robust performance across both EVA-CLIP and OpenAI-CLIP, consistently achieving significant improvements over state-of-the-art methods.

## 6. CONCLUSION

In this paper, we systematically analyze the attention maps of CLIP and VFM, revealing that CLIP’s core limitation in dense perception tasks is that its image tokens cannot effectively aggregate information from semantically relevant regions. To address this issue, we propose DeCLIP, a novel unsupervised fine-tuning framework that enhances dense representations of CLIP via a decoupled feature enhancement strategy. Extensive experiments on more than six diverse OV dense perception benchmarks, spanning 2D, 3D, and video data, demonstrate that DeCLIP achieves significant improvements over the original CLIP and other state-of-the-art methods. These results highlight the potential of DeCLIP as a foundational model for OV dense perception tasks.

<sup>5</sup>Quantitative comparisons with AM-RADIO are not conducted owing to its lack of OVSS support, as discussed in GitHub issues #81, #55, and #42.

## REFERENCES

- [1] S. Ren, K. He, R. Girshick, and J. Sun, “Faster r-cnn: Towards real-time object detection with region proposal networks,” *Advances in neural information processing systems*, vol. 28, 2015.
- [2] S. Liu, F. Li, H. Zhang, X. Yang, X. Qi, H. Su, J. Zhu, and L. Zhang, “DAB-DETR: Dynamic anchor boxes are better queries for DETR,” in *International Conference on Learning Representations*, 2022. [Online]. Available: <https://openreview.net/forum?id=oMI9PjOb9Jl>
- [3] O. Ronneberger, P. Fischer, and T. Brox, “U-net: Convolutional networks for biomedical image segmentation,” in *Medical image computing and computer-assisted intervention—MICCAI 2015: 18th international conference, Munich, Germany, October 5-9, 2015, proceedings, part III 18*. Springer, 2015, pp. 234–241.
- [4] B. Cheng, I. Misra, A. G. Schwing, A. Kirillov, and R. Girdhar, “Masked-attention mask transformer for universal image segmentation,” in *Proceedings of the IEEE/CVF conference on computer vision and pattern recognition*, 2022, pp. 1290–1299.
- [5] F. Li, H. Zhang, H. Xu, S. Liu, L. Zhang, L. M. Ni, and H.-Y. Shum, “Mask dino: Towards a unified transformer-based framework for object detection and segmentation,” in *Proceedings of the IEEE/CVF Conference on Computer Vision and Pattern Recognition*, 2023, pp. 3041–3050.
- [6] F. Chen, H. Zhang, K. Hu, Y.-K. Huang, C. Zhu, and M. Savvides, “Enhanced training of query-based object detection via selective query recollection,” in *Proceedings of the IEEE/CVF Conference on Computer Vision and Pattern Recognition (CVPR)*, June 2023, pp. 23 756–23 765.
- [7] X. Zhu, W. Su, L. Lu, B. Li, X. Wang, and J. Dai, “Deformable detr: Deformable transformers for end-to-end object detection,” *arXiv preprint arXiv:2010.04159*, 2020.
- [8] A. Zareian, K. D. Rosa, D. H. Hu, and S.-F. Chang, “Open-vocabulary object detection using captions,” in *Proceedings of the IEEE/CVF Conference on Computer Vision and Pattern Recognition*, 2021, pp. 14 393–14 402.
- [9] S. Wu, W. Zhang, S. Jin, W. Liu, and C. C. Loy, “Aligning bag of regions for open-vocabulary object detection,” in *Proceedings of the IEEE/CVF Conference on Computer Vision and Pattern Recognition*, 2023, pp. 15 254–15 264.
- [10] X. Wu, F. Zhu, R. Zhao, and H. Li, “Cora: Adapting clip for open-vocabulary detection with region prompting and anchor pre-matching,” in *Proceedings of the IEEE/CVF conference on computer vision and pattern recognition*, 2023, pp. 7031–7040.
- [11] S. Cho, H. Shin, S. Hong, A. Arnab, P. H. Seo, and S. Kim, “Cat-seg: Cost aggregation for open-vocabulary semantic segmentation,” in *Proceedings of the IEEE/CVF Conference on Computer Vision and Pattern Recognition*, 2024, pp. 4113–4123.
- [12] A. Radford, J. W. Kim, C. Hallacy, A. Ramesh, G. Goh, S. Agarwal, G. Sastry, A. Askell, P. Mishkin, J. Clark, G. Krueger, and I. Sutskever, “Learning transferable visual models from natural language supervision,” in *Proceedings of the 38th International Conference on Machine Learning*, ser. Proceedings of Machine Learning Research, M. Meila and T. Zhang, Eds., vol. 139. PMLR, 18–24 Jul 2021, pp. 8748–8763.
- [13] Y. Li, H. Fan, R. Hu, C. Feichtenhofer, and K. He, “Scaling language-image pre-training via masking,” in *Proceedings of the IEEE/CVF Conference on Computer Vision and Pattern Recognition*, 2023, pp. 23 390–23 400.
- [14] S. Wu, W. Zhang, L. Xu, S. Jin, W. Liu, and C. C. Loy, “Clim: Contrastive language-image mosaic for region representation,” in *Proceedings of the AAAI Conference on Artificial Intelligence*, vol. 38, 2024, pp. 6117–6125.
- [15] S. Wu, W. Zhang, L. Xu, S. Jin, X. Li, W. Liu, and C. C. Loy, “CLIPSelf: Vision transformer distills itself for open-vocabulary dense prediction,” in *The Twelfth International Conference on Learning Representations*, 2024. [Online]. Available: <https://openreview.net/forum?id=DjzvJCRsVf>
- [16] Y. Zhong, J. Yang, P. Zhang, C. Li, N. Codella, L. H. Li, L. Zhou, X. Dai, L. Yuan, Y. Li *et al.*, “Regionclip: Region-based language-image pretraining,” in *Proceedings of the IEEE/CVF Conference on Computer Vision and Pattern Recognition*, 2022, pp. 16 793–16 803.
- [17] J. Wang, B. Chen, B. Kang, Y. Li, Y. Chen, W. Xian, and H. Chang, “Ov-dqo: Open-vocabulary detr with denoising text query training and open-world unknown objects supervision,” *arXiv preprint arXiv:2405.17913*, 2024.
- [18] X. Gu, T.-Y. Lin, W. Kuo, and Y. Cui, “Open-vocabulary object detection via vision and language knowledge distillation,” *arXiv preprint arXiv:2104.13921*, 2021.

- [19] W. Kuo, Y. Cui, X. Gu, A. Piergiovanni, and A. Angelova, “F-vlm: Open-vocabulary object detection upon frozen vision and language models,” *arXiv preprint arXiv:2209.15639*, 2022.
- [20] F. Liang, B. Wu, X. Dai, K. Li, Y. Zhao, H. Zhang, P. Zhang, P. Vajda, and D. Marculescu, “Open-vocabulary semantic segmentation with mask-adapted clip,” in *Proceedings of the IEEE/CVF Conference on Computer Vision and Pattern Recognition*, 2023, pp. 7061–7070.
- [21] R. Rombach, A. Blattmann, D. Lorenz, P. Esser, and B. Ommer, “High-resolution image synthesis with latent diffusion models,” in *Proceedings of the IEEE/CVF conference on computer vision and pattern recognition*, 2022, pp. 10684–10695.
- [22] C. Zhu and L. Chen, “A survey on open-vocabulary detection and segmentation: Past, present, and future,” *arXiv preprint arXiv:2307.09220*, 2023.
- [23] J. Wu, X. Li, S. Xu, H. Yuan, H. Ding, Y. Yang, X. Li, J. Zhang, Y. Tong, X. Jiang *et al.*, “Towards open vocabulary learning: A survey,” *IEEE Transactions on Pattern Analysis and Machine Intelligence*, vol. 46, no. 7, pp. 5092–5113, 2024.
- [24] L. Wang, Y. Liu, P. Du, Z. Ding, Y. Liao, Q. Qi, B. Chen, and S. Liu, “Object-aware distillation pyramid for open-vocabulary object detection,” in *Proceedings of the IEEE/CVF Conference on Computer Vision and Pattern Recognition*, 2023, pp. 11 186–11 196.
- [25] J. Xu, S. De Mello, S. Liu, W. Byeon, T. Breuel, J. Kautz, and X. Wang, “Groupvit: Semantic segmentation emerges from text supervision,” in *Proceedings of the IEEE/CVF Conference on Computer Vision and Pattern Recognition*, 2023, pp. 18 134–18 144.
- [26] G. Ghiasi, X. Gu, Y. Cui, and T.-Y. Lin, “Scaling open-vocabulary image segmentation with image-level labels,” in *European Conference on Computer Vision*. Springer, 2022, pp. 540–557.
- [27] S. Zhao, S. Schuster, L. Zhao, Z. Zhang, V. K. B. G. Y. Suh, M. Chandraker, and D. N. Metaxas, “Taming self-training for open-vocabulary object detection,” in *Proceedings of the IEEE/CVF Conference on Computer Vision and Pattern Recognition (CVPR)*, June 2024, pp. 13 938–13 947.
- [28] X. Zhou, R. Girdhar, A. Joulin, P. Krähenbühl, and I. Misra, “Detecting twenty-thousand classes using image-level supervision,” in *European Conference on Computer Vision*. Springer, 2022, pp. 350–368.
- [29] Y. Zhang, W. Li, K. Zhou, C. Huang, and C. C. Loy, “Open-vocabulary detr with conditional matching,” in *European Conference on Computer Vision*. Springer, 2022, pp. 106–122.
- [30] K. Han, Y. Liu, J. H. Liew, H. Ding, J. Liu, Y. Wang, Y. Tang, Y. Yang, J. Feng, Y. Zhao *et al.*, “Global knowledge calibration for fast open-vocabulary segmentation,” in *Proceedings of the IEEE/CVF International Conference on Computer Vision*, 2023, pp. 797–807.
- [31] H. Zheng, H. Shi, Q. Peng, Y. X. Chng, R. Huang, Y. Weng, Z. Shi, and G. Huang, “Densegrounding: Improving dense language-vision semantics for ego-centric 3d visual grounding,” *arXiv preprint arXiv:2505.04965*, 2025.
- [32] H. Zhang, H. Jiang, Q. Yao, Y. Sun, R. Zhang, H. Zhao, H. Li, H. Zhu, and Z. Yang, “Detect anything 3d in the wild,” *arXiv preprint arXiv:2504.07958*, 2025.
- [33] Y. Yang, X. Wu, T. He, H. Zhao, and X. Liu, “Sam3d: Segment anything in 3d scenes,” *arXiv preprint arXiv:2306.03908*, 2023.
- [34] S. Lu, H. Chang, E. P. Jing, A. Boularias, and K. Bekris, “Ovir-3d: Open-vocabulary 3d instance retrieval without training on 3d data,” in *Conference on Robot Learning*. PMLR, 2023, pp. 1610–1620.
- [35] J. Corsetti, D. Boscaini, C. Oh, A. Cavallaro, and F. Poiesi, “Open-vocabulary object 6d pose estimation,” in *Proceedings of the IEEE/CVF Conference on Computer Vision and Pattern Recognition*, 2024, pp. 18 071–18 080.
- [36] P. Nguyen, T. D. Ngo, E. Kalogerakis, C. Gan, A. Tran, C. Pham, and K. Nguyen, “Open3dis: Open-vocabulary 3d instance segmentation with 2d mask guidance,” in *Proceedings of the IEEE/CVF Conference on Computer Vision and Pattern Recognition*, 2024, pp. 4018–4028.
- [37] A. Takmaz, E. Fedele, R. W. Sumner, M. Pollefeys, F. Tombari, and F. Engelmann, “Openmask3d: Open-vocabulary 3d instance segmentation,” *arXiv preprint arXiv:2306.13631*, 2023.
- [38] W. Zhu, J. Cao, J. Xie, S. Yang, and Y. Pang, “Clip-vis: Adapting clip for open-vocabulary video instance segmentation,” *IEEE Transactions on Circuits and Systems for Video Technology*, 2024.
- [39] F. Pan, H. Fang, F. Li, Y. Xu, Y. Li, L. Benini, and X. Lu, “Semantic and sequential alignment for referring video object segmentation,” in *Proceedings of the Computer Vision and Pattern Recognition Conference*, 2025, pp. 19 067–19 076.
- [40] H. Fang, P. Wu, Y. Li, X. Zhang, and X. Lu, “Unified embedding alignment for open-vocabulary video instance segmentation,” in *European Conference on Computer Vision*. Springer, 2024, pp. 225–241.
- [41] X. Zhai, B. Mustafa, A. Kolesnikov, and L. Beyer, “Sigmoid loss for language image pre-training,” in *Proceedings of the IEEE/CVF international conference on computer vision*, 2023, pp. 11 975–11 986.
- [42] S. Jiao, Y. Wei, Y. Wang, Y. Zhao, and H. Shi, “Learning mask-aware clip representations for zero-shot segmentation,” *Advances in Neural Information Processing Systems*, vol. 36, pp. 35 631–35 653, 2023.
- [43] B. Li, K. Q. Weinberger, S. Belongie, V. Koltun, and R. Ranftl, “Language-driven semantic segmentation,” *arXiv preprint arXiv:2201.03546*, 2022.
- [44] J. Mukhoti, T.-Y. Lin, O. Poursaeed, R. Wang, A. Shah, P. H. Torr, and S.-N. Lim, “Open vocabulary semantic segmentation with patch aligned contrastive learning,” in *Proceedings of the IEEE/CVF Conference on Computer Vision and Pattern Recognition*, 2023, pp. 19 413–19 423.
- [45] H. Wang, P. K. A. Vasu, F. Faghri, R. Vemulapalli, M. Farajtabar, S. Mehta, M. Rastegari, O. Tuzel, and H. Pouransari, “Sam-clip: Merging vision foundation models towards semantic and spatial understanding,” in *Proceedings of the IEEE/CVF Conference on Computer Vision and Pattern Recognition*, 2024, pp. 3635–3647.
- [46] H. Yuan, X. Li, C. Zhou, Y. Li, K. Chen, and C. C. Loy, “Open-vocabulary sam: Segment and recognize twenty-thousand classes interactively,” in *ECCV*, 2024.
- [47] X. Chen, H. Yang, S. Jin, X. Zhu, and H. Yao, “Frozensseg: Harmonizing frozen foundation models for open-vocabulary segmentation,” *arXiv preprint arXiv:2409.03525*, 2024.
- [48] A. Kirillov, E. Mintun, N. Ravi, H. Mao, C. Rolland, L. Gustafson, T. Xiao, S. Whitehead, A. C. Berg, W.-Y. Lo *et al.*, “Segment anything,” in *Proceedings of the IEEE/CVF International Conference on Computer Vision*, 2023, pp. 4015–4026.
- [49] S. Yu, S. Kwak, H. Jang, J. Jeong, J. Huang, J. Shin, and S. Xie, “Representation alignment for generation: Training diffusion transformers is easier than you think,” *arXiv preprint arXiv:2410.06940*, 2024.
- [50] Z. Liu, H. Mao, C.-Y. Wu, C. Feichtenhofer, T. Darrell, and S. Xie, “A convnet for the 2020s,” *Proceedings of the IEEE/CVF Conference on Computer Vision and Pattern Recognition (CVPR)*, 2022.
- [51] K. He, X. Zhang, S. Ren, and J. Sun, “Deep residual learning for image recognition,” in *Proceedings of the IEEE conference on computer vision and pattern recognition*, 2016, pp. 770–778.
- [52] A. Dosovitskiy, “An image is worth 16x16 words: Transformers for image recognition at scale,” *arXiv preprint arXiv:2010.11929*, 2020.
- [53] A. Vaswani, “Attention is all you need,” *Advances in Neural Information Processing Systems*, 2017.
- [54] M. Caron, H. Touvron, I. Misra, H. Jégou, J. Mairal, P. Bojanowski, and A. Joulin, “Emerging properties in self-supervised vision transformers,” in *Proceedings of the IEEE/CVF international conference on computer vision*, 2021, pp. 9650–9660.
- [55] M. Oquab, T. Darcet, T. Moutakanni, H. Vo, M. Szafraniec, V. Khalidov, P. Fernandez, D. Haziza, F. Massa, A. El-Nouby *et al.*, “Dinov2: Learning robust visual features without supervision,” *arXiv preprint arXiv:2304.07193*, 2023.
- [56] N. Ravi, V. Gabeur, Y.-T. Hu, R. Hu, C. Ryali, T. Ma, H. Khedr, R. Rädle, C. Rolland, L. Gustafson *et al.*, “Sam 2: Segment anything in images and videos,” *arXiv preprint arXiv:2408.00714*, 2024.
- [57] F. Wang, J. Mei, and A. Yuille, “Sclip: Rethinking self-attention for dense vision-language inference,” *arXiv preprint arXiv:2312.01597*, 2023.
- [58] T. Shao, Z. Tian, H. Zhao, and J. Su, “Explore the potential of clip for training-free open vocabulary semantic segmentation,” in *European Conference on Computer Vision*. Springer, 2025, pp. 139–156.
- [59] M. Lan, C. Chen, Y. Ke, X. Wang, L. Feng, and W. Zhang, “Clearclip: Decomposing clip representations for dense vision-language inference,” *arXiv preprint arXiv:2407.12442*, 2024.
- [60] M. Wyszczkańska, O. Siméoni, M. Ramamonjisoa, A. Bursuc, T. Trzciński, and P. Pérez, “Clip-dinoiser: Teaching clip a few dino tricks,” *arXiv preprint arXiv:2312.12359*, 2023.
- [61] J. Wang, X. Li, J. Zhang, Q. Xu, Q. Zhou, Q. Yu, L. Sheng, and D. Xu, “Diffusion model is secretly a training-free open vocabulary semantic segmenter,” *IEEE Transactions on Image Processing*, 2025.
- [62] K. Wang, F. Yang, S. Yang, M. A. Butt, and J. van de Weijer, “Dynamic prompt learning: Addressing cross-attention leakage for text-based image editing,” *Advances in Neural Information Processing Systems*, vol. 36, 2023.
- [63] L. Sun, J. Cao, J. Xie, X. Jiang, and Y. Pang, “Cliper: Hierarchically improving spatial representation of clip for open-vocabulary semantic segmentation,” *arXiv preprint arXiv:2411.13836*, 2024.
- [64] M. F. Naeem, Y. Xian, X. Zhai, L. Hoyer, L. Van Gool, and F. Tombari, “Silc: Improving vision language pretraining with self-distillation,” in *European Conference on Computer Vision*. Springer, 2025, pp. 38–55.



- [65] J. Chen, D. Zhu, G. Qian, B. Ghanem, Z. Yan, C. Zhu, F. Xiao, S. C. Culatana, and M. Elhoseiny, "Exploring open-vocabulary semantic segmentation from clip vision encoder distillation only," in *Proceedings of the IEEE/CVF International Conference on Computer Vision*, 2023, pp. 699–710.
- [66] K. He, G. Gkioxari, P. Dollár, and R. Girshick, "Mask r-cnn," in *Proceedings of the IEEE international conference on computer vision*, 2017, pp. 2961–2969.
- [67] W. Park, D. Kim, Y. Lu, and M. Cho, "Relational knowledge distillation," in *Proceedings of the IEEE/CVF conference on computer vision and pattern recognition*, 2019, pp. 3967–3976.
- [68] T.-Y. Lin, M. Maire, S. Belongie, J. Hays, P. Perona, D. Ramanan, P. Dollár, and C. L. Zitnick, "Microsoft coco: Common objects in context," in *Computer Vision—ECCV 2014: 13th European Conference, Zurich, Switzerland, September 6–12, 2014, Proceedings, Part V 13*. Springer, 2014, pp. 740–755.
- [69] I. Loshchilov, "Decoupled weight decay regularization," *arXiv preprint arXiv:1711.05101*, 2017.
- [70] Q. Sun, Y. Fang, L. Wu, X. Wang, and Y. Cao, "Eva-clip: Improved training techniques for clip at scale," *arXiv preprint arXiv:2303.15389*, 2023.
- [71] T. Darcet, M. Oquab, J. Mairal, and P. Bojanowski, "Vision transformers need registers," *arXiv preprint arXiv:2309.16588*, 2023.
- [72] D. Rozenberszki, O. Litany, and A. Dai, "Language-grounded indoor 3d semantic segmentation in the wild," in *European Conference on Computer Vision*. Springer, 2022, pp. 125–141.
- [73] T. D. Ngo, B.-S. Hua, and K. Nguyen, "Isbnnet: a 3d point cloud instance segmentation network with instance-aware sampling and box-aware dynamic convolution," in *Proceedings of the IEEE/CVF Conference on Computer Vision and Pattern Recognition*, 2023, pp. 13 550–13 559.
- [74] J. Schult, F. Engelmann, A. Hermans, O. Litany, S. Tang, and B. Leibe, "Mask3d: Mask transformer for 3d semantic instance segmentation," in *2023 IEEE International Conference on Robotics and Automation (ICRA)*. IEEE, 2023, pp. 8216–8223.
- [75] S. Peng, K. Genova, C. Jiang, A. Tagliasacchi, M. Pollefeys, T. Funkhouser *et al.*, "Opensecene: 3d scene understanding with open vocabularies," in *Proceedings of the IEEE/CVF conference on computer vision and pattern recognition*, 2023, pp. 815–824.
- [76] M. Ester, H.-P. Kriegel, J. Sander, X. Xu *et al.*, "A density-based algorithm for discovering clusters in large spatial databases with noise," in *kdd*, vol. 96, no. 34, 1996, pp. 226–231.
- [77] Z. Huang, X. Wu, X. Chen, H. Zhao, L. Zhu, and J. Lasenby, "Openins3d: Snap and lookup for 3d open-vocabulary instance segmentation," in *European Conference on Computer Vision*. Springer, 2024, pp. 169–185.
- [78] L. Yang, Y. Fan, and N. Xu, "Video instance segmentation," in *Proceedings of the IEEE/CVF international conference on computer vision*, 2019, pp. 5188–5197.
- [79] J. Wu, Q. Liu, Y. Jiang, S. Bai, A. Yuille, and X. Bai, "In defense of on-line models for video instance segmentation," in *European Conference on Computer Vision*. Springer, 2022, pp. 588–605.
- [80] A. Bewley, Z. Ge, L. Ott, F. Ramos, and B. Upcroft, "Simple online and realtime tracking," in *2016 IEEE international conference on image processing (ICIP)*. IEEE, 2016, pp. 3464–3468.
- [81] Y. Liu, I. E. Zulfikar, J. Luiten, A. Dave, D. Ramanan, B. Leibe, A. Osep, and L. Leal-Taixé, "Opening up open world tracking," in *Proceedings of the IEEE/CVF conference on computer vision and pattern recognition*, 2022, pp. 19 045–19 055.
- [82] H. K. Cheng and A. G. Schwing, "Xmem: Long-term video object segmentation with an atkinson-shiffrin memory model," in *European Conference on Computer Vision*. Springer, 2022, pp. 640–658.
- [83] H. Wang, C. Yan, S. Wang, X. Jiang, X. Tang, Y. Hu, W. Xie, and E. Gavves, "Towards open-vocabulary video instance segmentation," in *proceedings of the IEEE/CVF international conference on computer vision*, 2023, pp. 4057–4066.
- [84] L. Yang, Y. Fan, and N. Xu, "Video instance segmentation," in *Proceedings of the IEEE/CVF international conference on computer vision*, 2019, pp. 5188–5197.
- [85] A. Gupta, P. Dollar, and R. Girshick, "Lvis: A dataset for large vocabulary instance segmentation," in *Proceedings of the IEEE/CVF conference on computer vision and pattern recognition*, 2019, pp. 5356–5364.
- [86] J. Qi, Y. Gao, Y. Hu, X. Wang, X. Liu, X. Bai, S. Belongie, A. Yuille, P. H. Torr, and S. Bai, "Occluded video instance segmentation: A benchmark," *International Journal of Computer Vision*, vol. 130, no. 8, pp. 2022–2039, 2022.
- [87] A. Athar, J. Luiten, P. Voigtlaender, T. Khurana, A. Dave, B. Leibe, and D. Ramanan, "Burst: A benchmark for unifying object recognition, segmentation and tracking in video," in *Proceedings of the IEEE/CVF winter conference on applications of computer vision*, 2023, pp. 1674–1683.
- [88] Y. He, Y. Wang, H. Fan, J. Sun, and Q. Chen, "Fs6d: Few-shot 6d pose estimation of novel objects," in *Proceedings of the IEEE/CVF Conference on Computer Vision and Pattern Recognition*, 2022, pp. 6814–6824.
- [89] M. Savva, A. X. Chang, and P. Hanrahan, "Semantically-enriched 3d models for common-sense knowledge," in *Proceedings of the IEEE Conference on Computer Vision and Pattern Recognition Workshops*, 2015, pp. 24–31.
- [90] H. Wang, S. Sridhar, J. Huang, J. Valentin, S. Song, and L. J. Guibas, "Normalized object coordinate space for category-level 6d object pose and size estimation," in *Proceedings of the IEEE/CVF conference on computer vision and pattern recognition*, 2019, pp. 2642–2651.
- [91] T. Hodan, F. Michel, E. Brachmann, W. Kehl, A. GlentBuch, D. Kraft, B. Drost, J. Vidal, S. Ihrke, X. Zabulis *et al.*, "Bop: Benchmark for 6d object pose estimation," in *Proceedings of the European conference on computer vision (ECCV)*, 2018, pp. 19–34.
- [92] T. Hodaň, M. Sundermeyer, B. Drost, Y. Labbé, E. Brachmann, F. Michel, C. Rother, and J. Matas, "Bop challenge 2020 on 6d object localization," in *Computer Vision—ECCV 2020 Workshops: Glasgow, UK, August 23–28, 2020, Proceedings, Part II 16*. Springer, 2020, pp. 577–594.
- [93] Z. Liu, Y. Lin, Y. Cao, H. Hu, Y. Wei, Z. Zhang, S. Lin, and B. Guo, "Swin transformer: Hierarchical vision transformer using shifted windows," in *Proceedings of the IEEE/CVF international conference on computer vision*, 2021, pp. 10 012–10 022.
- [94] N. Carion, F. Massa, G. Synnaeve, N. Usunier, A. Kirillov, and S. Zagoruyko, "End-to-end object detection with transformers," in *European conference on computer vision*. Springer, 2020, pp. 213–229.
- [95] D. Kim, A. Angelova, and W. Kuo, "Region-aware pretraining for open-vocabulary object detection with vision transformers," in *Proceedings of the IEEE/CVF Conference on Computer Vision and Pattern Recognition*, 2023, pp. 11 144–11 154.
- [96] —, "Contrastive feature masking open-vocabulary vision transformer," in *2023 IEEE/CVF International Conference on Computer Vision (ICCV)*, 2023, pp. 15 556–15 566.
- [97] J. Ding, N. Xue, G.-S. Xia, and D. Dai, "Decoupling zero-shot semantic segmentation," in *Proceedings of the IEEE/CVF Conference on Computer Vision and Pattern Recognition*, 2022, pp. 11 583–11 592.
- [98] M. Xu, Z. Zhang, F. Wei, Y. Lin, Y. Cao, H. Hu, and X. Bai, "A simple baseline for open-vocabulary semantic segmentation with pre-trained vision-language model," in *European Conference on Computer Vision*. Springer, 2022, pp. 736–753.
- [99] M. Xu, Z. Zhang, F. Wei, H. Hu, and X. Bai, "Side adapter network for open-vocabulary semantic segmentation," in *Proceedings of the IEEE/CVF Conference on Computer Vision and Pattern Recognition*, 2023, pp. 2945–2954.
- [100] J. Xu, S. Liu, A. Vahdat, W. Byeon, X. Wang, and S. De Mello, "Open-vocabulary panoptic segmentation with text-to-image diffusion models," in *Proceedings of the IEEE/CVF Conference on Computer Vision and Pattern Recognition*, 2023, pp. 2955–2966.
- [101] Q. Yu, J. He, X. Deng, X. Shen, and L.-C. Chen, "Convolutions die hard: Open-vocabulary segmentation with single frozen convolutional clip," *Advances in Neural Information Processing Systems*, vol. 36, 2024.
- [102] C. Zhou, C. C. Loy, and B. Dai, "Extract free dense labels from clip," in *European Conference on Computer Vision*. Springer, 2022, pp. 696–712.
- [103] G. Shin, W. Xie, and S. Albanie, "Reco: Retrieve and co-segment for zero-shot transfer," *Advances in Neural Information Processing Systems*, vol. 35, pp. 33 754–33 767, 2022.
- [104] J. Cha, J. Mun, and B. Roh, "Learning to generate text-grounded mask for open-world semantic segmentation from only image-text pairs," in *Proceedings of the IEEE/CVF Conference on Computer Vision and Pattern Recognition*, 2023, pp. 11 165–11 174.
- [105] S. Hajimiri, I. Ben Ayed, and J. Dolz, "Pay attention to your neighbours: Training-free open-vocabulary semantic segmentation," in *Proceedings of the IEEE/CVF Winter Conference on Applications of Computer Vision*, 2025.
- [106] Y. Yang, J. Deng, W. Li, and L. Duan, "Resclip: Residual attention for training-free dense vision-language inference," in *Proceedings of*

- the Computer Vision and Pattern Recognition Conference*, 2025, pp. 29 968–29 978.
- [107] M. Lan, C. Chen, Y. Ke, X. Wang, L. Feng, and W. Zhang, “Proxyclip: Proxy attention improves clip for open-vocabulary segmentation,” in *European Conference on Computer Vision*. Springer, 2024, pp. 70–88.
  - [108] H. Caesar, J. Uijlings, and V. Ferrari, “Coco-stuff: Thing and stuff classes in context,” in *Proceedings of the IEEE conference on computer vision and pattern recognition*, 2018, pp. 1209–1218.
  - [109] B. Zhou, H. Zhao, X. Puig, T. Xiao, S. Fidler, A. Barriuso, and A. Torralba, “Semantic understanding of scenes through the ade20k dataset,” *International Journal of Computer Vision*, vol. 127, pp. 302–321, 2019.
  - [110] M. Everingham, L. Van Gool, C. K. Williams, J. Winn, and A. Zisserman, “The pascal visual object classes (voc) challenge,” *International journal of computer vision*, vol. 88, pp. 303–338, 2010.
  - [111] R. Mottaghi, X. Chen, X. Liu, N.-G. Cho, S.-W. Lee, S. Fidler, R. Urtasun, and A. Yuille, “The role of context for object detection and semantic segmentation in the wild,” in *Proceedings of the IEEE conference on computer vision and pattern recognition*, 2014, pp. 891–898.
  - [112] J. Ding, N. Xue, G.-S. Xia, and D. Dai, “Decoupling zero-shot semantic segmentation,” in *Proceedings of the IEEE/CVF Conference on Computer Vision and Pattern Recognition*, 2022, pp. 11 583–11 592.
  - [113] M. Cordts, M. Omran, S. Ramos, T. Rehfeld, M. Enzweiler, R. Benenson, U. Franke, S. Roth, and B. Schiele, “The cityscapes dataset for semantic urban scene understanding,” in *Proceedings of the IEEE conference on computer vision and pattern recognition*, 2016, pp. 3213–3223.
  - [114] C. Qiu, Y. Wu, W. Ke, X. Bai, and T. Zhang, “Refining clip’s spatial awareness: A visual-centric perspective,” *arXiv preprint arXiv:2504.02328*, 2025.
  - [115] A. Kirillov, K. He, R. Girshick, C. Rother, and P. Dollár, “Panoptic segmentation,” in *Proceedings of the IEEE/CVF conference on computer vision and pattern recognition*, 2019, pp. 9404–9413.
  - [116] M. Ranzinger, G. Heinrich, J. Kautz, and P. Molchanov, “Am-radio: Agglomerative vision foundation model reduce all domains into one,” in *Proceedings of the IEEE/CVF Conference on Computer Vision and Pattern Recognition*, 2024, pp. 12 490–12 500.
  - [117] J. Zhang, C. Herrmann, J. Hur, L. Polania Cabrera, V. Jampani, D. Sun, and M.-H. Yang, “A tale of two features: Stable diffusion complements dino for zero-shot semantic correspondence,” *Advances in Neural Information Processing Systems*, vol. 36, pp. 45 533–45 547, 2023.
  - [118] P. Sharma, N. Ding, S. Goodman, and R. Soricut, “Conceptual captions: A cleaned, hypernymed, image alt-text dataset for automatic image captioning,” in *Proceedings of the 56th Annual Meeting of the Association for Computational Linguistics (Volume 1: Long Papers)*, 2018, pp. 2556–2565.